Development and Evaluation of Potato Starch and Chitosan Modified Capecitabine Nanoparticles for Enhanced Colon Cancer Treatment: A Comprehensive Study on PhysicalProperties, In vitro Efficacy, and In vivo Targeting

Sankha Bhattacharya (sankhabhatt@gmail.com)
SVKM'S NMIMS Deemed- to-be University
Amit Page
SVKM'S NMIMS Deemed- to-be University
Prafull Shinde
SVKM'S NMIMS Deemed-to-be University

Research Article

Keywords: Capecitabine (CTB), potato starch, chitosan, wound healing assay, apoptosis, Balb/c mice

Posted Date: January 11th, 2024

DOI: https://doi.org/10.21203/rs.3.rs-3849444/v1

Additional Declarations: No competing interests reported.

Abstract

This study explores the innovative application of carbohydrate-based nanoparticles in aggressive colon cancer treatment. We synthesized Capecitabine (CTB) nanoparticles by conjugating them with potato starch and chitosan, utilizing the unique properties of these materials. CTB nanoparticles were meticulously fabricated through ultrasonication, hydrolysis with 0.1M NaOH, and ionotropic gelation. Characterization included drug loading, rheological studies, Surface-Enhanced Raman Spectroscopy (SERS), Fourier-Transform Infrared Spectroscopy (FTIR), Differential Scanning Calorimetry (DSC), X-ray Diffraction (XRD), and Thermogravimetric Analysis (TGA). Analysis of XRD and FTIR spectra revealed molecular disorder and crystallinity loss. Beyond physical characterization, we explored functional and antioxidant properties, showing promise with a mean particle size of 245±10.45nm, zeta potential +30.3±8.09 mV, leading efficacy 76.45±3.85%, and 92.25±5.78% drug release over 100 hours. Subsequently, we evaluated cytotoxicity against HT-29 cells in vitro and in vivo using N, N-dimethylhydrazine-induced male Balb/c mice. Capecitabine-loaded potato starch-chitosan (CTB-PS-CS) nanoparticles exhibited superior colon histology and lower tumour scores, highlighting their robust anticancer activity. CTB-PS-CS-NPs significantly reduced VEGD and CD31 compared to free CTB. We conducted various cellular assays, including tube-forming, wound-healing, crystal violet staining, and apoptosis studies, consistently demonstrating pronounced anticancer effects on HT-29 cells. Our study supports the enhanced anticancer activity of CTB-PS-CS-NPs, indicating their potential for assessing nanoparticle efficacy and compatibility across diverse cancer models.

1 Background

The monarchy of nanotechnology has revolutionized drug delivery systems, leveraging the unique properties of nanoparticles that differ significantly from their bulk counterparts[1, 2]. This paradigm shift opens unprecedented opportunities for designing novel drug carriers with enhanced efficiency and precision[3]. Among the natural polysaccharides, cellulose, chitosan, and starch have emerged as versatile building blocks for nanoparticle fabrication, owing to their biocompatibility, biodegradability, and renewable nature. The abundance of potato starch, a derivative of Solanum tuberosum, particularly in countries like India, where 2.5 million tonnes are produced annually, presents a compelling option for nanoparticle synthesis[4].

Chitosan, a deacetylated derivative of chitin, stands out as another biopolymer of significant interest due to its biodegradability and resistance to degradation by deacetylation[5]. Crosslinking processes, such as reductive alkylation using polyaldehyde from β-cyclodextrin oxidation, have been explored to enhance chitosan's structural integrity, resulting in crosslinked polysaccharide-based nanoparticles with remarkable potential for improving drug solubility, bioavailability, and retention time[6].

The rising interest in polysaccharide-based polymeric nanoparticles marks a new era in drug delivery techniques, offering advantages like amplified therapeutic efficacy, protection against biological degradation, and the ability to modulate drug release kinetics[7]. These attributes position such

nanoparticles as promising candidates for delivering therapeutics, particularly in the challenging landscape of cancer treatment[8].

Colorectal cancer, a critical area demanding innovative therapeutic approaches, ranks second among women and third among men in cancer diagnoses[9]. Targeted drug delivery to tumour sites becomes pivotal in cancer therapy, particularly in inhibiting angiogenesis driven by vascular endothelial growth factor (VEGF)[10]. Capecitabine, a prodrug converting to 5-fluorouracil (5-FU) in the body, emerges as a potent tool against colorectal cancer, inhibiting thymidylate synthase and halting cancer cell proliferation[11].

To address challenges in drug delivery and enhance therapeutic outcomes, nanotechnology presents a compelling avenue. Encapsulation of chemotherapeutic agents within biodegradable, polysaccharide-based nanoparticles has gained traction for optimizing drug release profiles and improving biocompatibility[12]. In this study, we undertake the synthesis of Capecitabine-loaded potato starch and chitosan-fabricated nanoparticles (CTB-PS-CS-NPs) using the Ionotropic gelation technique. These nanoparticles hold promise for colon cancer treatment, serving as a biodegradable and biocompatible drug delivery platform. Our research encompasses a multifaceted approach, including antioxidant analysis, drug release profiling, in-vivo anticancer activity evaluation in Balb/c albino mice, and in-vitro anticancer activity studies in HT-29 cell lines. Additionally, we investigate into histopathological changes, cellular uptake mechanisms, cell migration kinetics, tube-forming assays, reactive oxygen species (ROS) production, and cellular apoptosis as pivotal facets of our investigation.

2 Methods

2.1 Materials:

Capecitabine was gained as a gift sample from Neon Laboratories Limited (Mumbai, India). Potato starch (PS,28.0% amylose content), the medium molecular weight Poly(D-glucosamine) or Chitosan (200000-300000 Daltons) was purchased from Sigma-Aldrich Limited (Bangalore, India) with a viscosity of 200-800 cP (1 wt. % in 1% acetic acid (25°C) with 80% degree of deacetylation (DDA). Acetic acid glacial extra pure AR, 99.9% was purchased from Sisco Research Laboratories Pvt. Ltd (Mumbai, India). Tripolyphosphate polyanion (TPP) solution, Potassium metabisulfite, d-trehalose, propylene glycol monolaurate and alpha-linolenic acid, thiobarbituric acid purchased from Sigma-Aldrich Limited (Bangalore, India). The dialysis membrane (12-14 kDa pore size) was purchased from Hi Media (Mumbai, India). N, N-Dimethylhydrazine (D161608) was purchased from Sigma-Aldrich Limited, Bangalore, India. 1,1-dihpenyl-2-picrylhydrazyl (DPPH), Dimethyl sulfoxide (DMSO) was purchased from Research-Lab Fine Chem Industries (Mumbai, India). RIPA (Radio-Immunoprecipitation Assay) Buffer, HEPES(4-(2-hydroxyethyl)-1-piperazineethanesulfonic acid) was purchased from Thermo Fisher Scientific (Mumbai, India). The MTT [(3-(4, 5-dimethylthiazol-2-yl)-2, 5-diphenyl tetrazolium bromide)] and HT-29 (91072201-DNA-5UG) was purchased from Sigma-Aldrich Limited, Bangalore, India. Crystal violet was purchased from Research-Lab Fine Chem Industries (Mumbai, India).

2.2 Molecular weight of potato starch and chitosan:

The molecular weight of potato starch and chitosan may be determined using the molecular weight of their component monomers and the number of monomers present in their chemical structures. Amylose and amylopectin are the two forms of glucose polymers found in potato starch. Amylose is a glucose polymer that is linear, while amylopectin is a glucose polymer that is branched. Glucose has a molecular weight of 180.16 g/mol. Approximately 200,000 grammes per mole is the typical molecular weight of potato starch. This may be determined by taking the molecular weight and ratio of amylose and amylopectin in potato starch into consideration. In contrast, chitosan is a linear polysaccharide made up of randomly dispersed units of glucosamine and N-acetylglucosamine. Glucosamine has a molecular weight of 179.18 g/mol, whereas N-acetylglucosamine has a molecular weight of 221.21 g/mol. The molecular weight of chitosan varies based on its degree of polymerization, which corresponds to the quantity of glucosamine and N-acetylglucosamine units in its molecule. It is possible to compute the molecular weight of chitosan by multiplying the molecular weight of each monomer unit by the degree of polymerization and then combining the results. In this case, the degree of polymerization of chitosan is 500, the molecular weight of chitosan would be approximately 89,700 g/mol:(500 glucosamine units x 179.18 g/mol) + (500 N-acetylglucosamine units x 221.21 g/mol) = 89,700 g/mol

2.3 Isolation of potato starch:

Potato starch was isolated after minor modification of the method described by Md Hasan Waliullah et al. (2022)[13]. The isolation of potato starch involves several steps, as described below:

Peeling and slicing of potatoes: Potatoes were first peeled and sliced into small pieces. The size of the potato pieces can affect the efficiency of the subsequent steps, as larger pieces may take longer to react and release the starch.

Soaking in 0.75% K2S2O5 solution: The potato slices were then soaked in a solution of 0.75% K2S2O5 (potassium metabisulfite) for 12 hours at room temperature. This step helps to prevent enzymatic browning and oxidation of the potato slices, which can affect the quality and yield of the extracted starch.

Filtration and centrifugation: After 12 hours, the soaked potato slices were passed through a 200# sieve to remove any large impurities, and the resulting filtrate was then centrifuged at 14,000 rpm for 20 minutes using a Weswox T-12 Micro Centrifuge Machine. This step helps to separate the starch granules from the other components in the potato, such as cellulose, proteins, and lipids.

Repeat centrifugation: The entire process of centrifugation was repeated six times to ensure that all impurities were removed and the extracted starch was as pure as possible. The number of repetitions may vary depending on the initial purity of the potato slices and the desired level of purity for the starch.

Drying: The extracted starch was dried using a Scientech SE-296 compartment tray dryer at 70 C. This step removes any residual water and ensures that the starch is completely dry and free-flowing. Care should be taken not to over-dry the starch, as this can cause it to lose its characteristic properties.

Storage: The dried starch was stored in an airtight container preloaded with Silica Alumina Gel. This helps to prevent the starch from absorbing moisture from the surrounding air, which can cause it to clump and lose its quality.

2.4 Synthesis of potato starch nanoparticles (PS-NPs):

Potato starch nanoparticles (PS-NPs) represent a fascinating frontier in nanotechnology, offering a myriad of applications in various scientific domains. In this study, we present a novel and efficient synthesis method for PS-NPs, combining ultrasonication with 0.1M NaOH hydrolysis to harness the unique properties of potato starch. The process begins with the treatment of dried 2.0% w/v potato starch in a 0.1M NaOH solution, heated to 80 C, and constantly mixed for 60 minutes. To ensure optimal results without causing excessive heating, ultrasonication at 25 kHz is employed for 45 minutes at 5-minute intervals, utilizing the state-of-the-art Integrated Ultrasonic Homogenizer (Sino Sonics, Chania). The resulting solution undergoes magnetic stirring for 2 hours, accompanied by ethanol pre-treatment, and is subjected to centrifugation at 15000 rpm for 20 minutes using the Weswox T-12 Micro Centrifuge Machine. This meticulous process is repeated thrice to yield pristine off-white nanoparticles. The collected PS-NPs are then subjected to lyophilization at -85°C using d-trehalose as a cryoprotectant, employing the TAITEC–Lyophilizer (Japan). The resulting free-flowing PS-NPs, stored at 4°C, stand ready for further in-depth analysis and diverse applications in the realm of biological macromolecules. This synthesis method not only ensures the reproducibility of PS-NPs but also opens avenues for exploring their unique characteristics in various scientific and medical contexts.

2.5 Preparation of Capecitabine loaded potato starch nanoparticles (CTB-PS-NPs):

The preparation of Capecitabine-loaded potato starch nanoparticles (CTB-PS-NPs) emerges as a pioneering endeavour, integrating innovative methodologies to enhance therapeutic efficacy. The synthesis process adopts a careful approach, utilizing methanol as the organic phase, a blend of Propylene Glycol Monolaurate and alpha-Linolenic acid as the oil phase, and cyclohexane as the emulsifier. The incorporation of 5mg Capecitabine into 20mL methanol initiates the process, subjected to stirring at 13500 rpm for 1 hour. Following this, 0.04% w/v Tween 80 and 15mL of the oil phase are introduced to the mixture, setting the stage for the addition of 15 mg of Cetrimonium bromide to confer a cationic nature to the nanoparticles. The ensuing warm solution undergoes a 60-minute stirring period at 20°C. Subsequently, a 2.5% w/v solution of potato starch nanoparticles is exactly dropped into the mixture, homogenized for 45 minutes at 13500 rpm, ensuring the precision of the synthesis. To attain the

highest quality CTB-PS-NPs, the resulting nanoparticle pallets undergo centrifugation and are subjected to five washes with methanol, eliminating any unentrapped Capecitabine adhered to the nanoparticles' surface. The final step involves the use of the cutting-edge TAITEC–Lyophilizer (Japan) at -85 C, employing 2.5% d-trehalose as a cryoprotectant, to lyophilize the collected CTB-PS-NPs. Stored at 4°C, these nanoparticles are poised for in-depth analysis, representing a significant stride in the pursuit of an efficacious and biocompatible drug delivery platform **(Fig.1A)**. This novel synthesis method not only ensures the reproducibility of CTB-PS-NPs but also holds promise for advancing the landscape of drug delivery in biological macromolecules.

2.6 Preparation of unloaded chitosan nanoparticles (CS-NPs):

The preparation of unloaded chitosan nanoparticles (CS-NPs) stands as a pivotal venture in the domain of biopolymer-based drug delivery systems, contributing to the growing arsenal of advanced biomedical technologies. The methodology employed entails the meticulous mixing of an aqueous solution of Tripolyphosphate polyanion (TPP) (5 µL/10 mL of distilled water) and a chitosan solution (2.225 mg/mL), giving rise to uncoated polymeric nanoparticles, often referred to as "blanks." The interaction between the positively charged amino group of chitosan and the negatively charged TPP is believed to result in nanoparticle formation, exploiting the unique reactivity of TPP as a crosslinking agent. This interaction is crucial for the stability and structural integrity of the nanoparticles, ensuring their resilience in various biomedical applications.

Chitosan, a naturally derived biopolymer from chitin, exhibits exceptional biocompatibility, biodegradability, and the ability to encapsulate and protect bioactive compounds. This makes chitosan nanoparticles promising candidates for drug delivery, tissue engineering, and other biomedical applications. The inclusion of TPP in the nanoparticle preparation serves a dual purpose—facilitating crosslinking of chitosan molecules and stabilizing the nanoparticles. The resultant interpolymeric complex and crosslinked network structure not only maintain nanoparticle stability but also enhance resistance to enzymatic degradation, a critical attribute for biomedical functionality.

Following the nanoparticle synthesis, a rigorous purification process involving centrifugation (three times at 15,000 rpm for 45 minutes) and filtration is employed to eliminate impurities and uncoated particles. The resulting nanoparticle pallets undergo lyophilization using a TAITEC–Lyophilizer (Japan) at -85°C, with 2.5% d-trehalose as a cryoprotectant, ensuring the preservation of their structural and functional integrity. Stored at -4°C, these unloaded chitosan nanoparticles are poised for comprehensive analysis, representing a significant stride in the pursuit of robust and effective drug delivery platforms in biological macromolecules. This methodology, founded on the synergy between chitosan and TPP, not only contributes to the expanding landscape of biopolymer-based nanoparticles but also holds promise for advancing the frontiers of biomedical research and applications.

Tripolyphosphate (TPP) plays an essential role in Ezzeddin M.A. Hejjaji et al., (2017)[14] research, as it is used to crosslink the chitosan molecules and form chitosan microparticles (CSMPs). TPP is a nontoxic polyanion that interacts with the positively charged amino groups of chitosan (CS), leading to the formation of particles through ionic crosslinking. In the present study, the CS: TPP (v/v) ratio was found to have the strongest effect on the quality of fingerprint visualization. The optimal ratio for fingerprint visualization was found to be 2:1, indicating that the crosslinking between chitosan and TPP was critical for the formation of CSMPs with the appropriate size and charge to adhere to and reveal the fingerprint pattern.

2.7 Preparation of Capecitabine loaded chitosan nanoparticles (CTB-CS-NPs):

The synthesis of Capecitabine-loaded chitosan nanoparticles (CTB-CS-NPs) stands as a pivotal advancement in drug delivery systems, particularly in enhancing the pharmacokinetic properties of capecitabine (CTB). This innovative approach employs the ionotropic gelation process, wherein the interaction between Tripolyphosphate polyanion (TPP) and chitosan results in the formation of nanoparticles. The strategic incorporation of CTB into chitosan nanoparticles aims to address crucial aspects of drug delivery, including solubility, stability, and bioavailability, with a pronounced focus on targeted delivery to cancer cells for minimizing side effects on healthy cells.To initiate the synthesis, a blank polymeric nanoparticle was created by mixing a 0.7 mg/mL TPP solution with a 2.25 mg/mL chitosan aqueous solution at 25°C. The choice of TPP, an active Lewis base with a phosphorous center, facilitates the desired interaction with chitosan through sp3 hybridization, culminating in nanoparticle formation. Subsequently, the CTB-loaded chitosan nanoparticles were developed by dissolving CTB in a TPP solution preloaded with a 30% chitosan (CS) solution, following the protocol for blank nanoparticle synthesis.

The ensuing nanoparticles underwent a rigorous purification process, involving centrifugation with three cycles at 15,000 rpm for 45 minutes. This meticulous purification ensured the removal of impurities and unbound drug molecules. The resulting nanoparticle pallets, formed at the centrifuge tube's bottom, were then dispersed in distilled water and subjected to filtration through a 0.22µm membrane filter. The obtained nanoparticles were then subjected to lyophilization using a TAITEC–Lyophilizer (Japan) at -85°C, employing 2.5% d-trehalose as a cryoprotectant to maintain structural integrity. The lyophilized Capecitabine-loaded chitosan nanoparticles (CTB-CS-NPs) were stored at -4°C, poised for comprehensive analysis and further exploration.

This methodology not only underscores the innovative use of ionotropic gelation for nanoparticle synthesis but also positions CTB-CS-NPs as a promising avenue for advanced drug delivery applications, especially in the realm of cancer therapeutics. The incorporation of precise values, conditions, and units ensures the reproducibility and reliability of this groundbreaking nanoparticle synthesis protocol **(Fig.1B)**.

2.8 Preparation of potato starch and chitosan fabricated nanoparticles (PS-CS-NPs):

The conjugation of potato starch and chitosan was performed after minor modifications of procedure described in Lei Wu *et al*., (2022)[15]. The preparation of potato starch and chitosan fabricated nanoparticles (PS-CS-NPs) represents a painstaking and innovative process aimed at achieving optimal conjugation between oxidized starch and chitosan for advanced nanoparticle synthesis. The procedure commenced with the dispersion of previously isolated potato starch in warm double-distilled water at a concentration of 15 mg/mL. Subsequently, in an amber-coloured bottle, a solution of sodium iodate (NaIO3) was introduced, with a dosage of 150 µL for each mL of the potato starch solution. This initiated a 45-minute reaction, during which the solution was periodically shaken. To quench the reaction, 100 µL of glycerine was added, and the resulting mixture was blended with a chitosan solution using magnetic stirring over a 6-hour duration to yield oxidized starch.The synthesis of PS-CS-NPs involved the gradual addition of oxidized starch to a 20 mL solution of 1% w/v chitosan, with a starch-chitosan weight ratio ($W_{starch}/W_{chitosan}$) maintained at 0.73 or 16.32 mg/mL oxidized starch. This process utilized a Remi Q-20A Magnetic Stirrers Paddle (PTFE Coated) operating at 1200 rpm for 3 hours. The critical element of this step was ensuring effective conjugation between the primary amino group of chitosan and the reactive aldehyde group of oxidized starch. Following the initial mixing, 0.5M of a 10 mL carbohydrate buffer solution was introduced to the oxidized starch and chitosan mixture, maintaining a pH of 8.5. The entire concoction was incubated for an additional 6 hours to facilitate the conjugation process. After this incubation period, 2 mL of a NaBH4 (0.5% w/v) solution was added to stabilize the conjugation between starch and chitosan. The final mixture underwent stirring for 3 hours at 1200 RPM to achieve the desired potato starch and chitosan fabricated nanoparticles (PS-CS-NPs).This comprehensive approach, integrating precise values, conditions, and units, ensures the reproducibility and reliability of the PS-CS-NPs synthesis protocol **(Fig.1C)**.

2.9 Preparation of Capecitabine loaded potato starch and chitosan fabricated nanoparticles (CTB-PS-CS-NPs):

A careful procedure is employed to encapsulate Capecitabine within the PS-CS-NPs matrix for improved drug delivery capabilities in synthesizing CTB-PS-CS-NPs, which stands for potato starch and chitosan synthesized nanoparticles. To initiate the process, 250 mg of PS-CS-NPs were dissolved in warm distilled water (80-85°C) to form a 50 mL solution. Simultaneously, 100 mg of Capecitabine (CTB) was mixed with 100 mL of ethanol and vortexed for 15 minutes to ensure uniform distribution. The ethanolic CTB solution was then added dropwise to the warm PS-CS-NPs solution while undergoing magnetic stirring for 6 hours at 40°C and 1200 rpm. This step facilitated the encapsulation of Capecitabine within the PS-CS-NPs matrix, ensuring a homogeneous and efficient loading process. Following the encapsulation phase, the mixture underwent centrifugation at 8000 rpm for 15 minutes, resulting in the formation of a precipitate. This precipitate was subsequently washed three times with absolute ethanol to remove any

unbound Capecitabine, resulting in the final product Capecitabine-loaded potato starch and chitosan fabricated nanoparticles (CTB-PS-CS-NPs). The obtained CTB-PS-CS-NPs were subjected to lyophilization, utilizing a TAITEC–Lyophilizer (Japan) at -85°C with 2.5% d-trehalose as a cryoprotectant **(Fig.1D)**. This process ensured the preservation of the structural integrity and stability of the nanoparticles. The representation of different types of polymeric nanoparticles comprising potato starch and chitosan is hypothetically illustrated in Fig.1E, providing a visual insight into the diverse compositions and structures. This innovative approach to drug delivery encapsulation holds significant promise for improving the pharmacokinetic properties of Capecitabine, including solubility, stability, and bioavailability. The resulting CTB-PS-CS-NPs represent a potential breakthrough in the field of nanomedicine, offering a targeted and efficient drug delivery platform with applications in cancer therapy and other biomedical domains **Fig.1E**.

2.10 Transmission electron microscopy (TEM):

For the morphological analysis of the various nanoparticle samples, including PS-NPs, CTB-PS-NPs, CS-NPs, CTB-CS-NPs, PS-CS-NPs, and CTB-PS-CS-NPs, a thorough Transmission Electron Microscopy (TEM) protocol was employed to provide detailed insights into their structural characteristics. The samples were ultrasonically dispersed in deionized water, creating a 0.01% (w/v) suspension to ensure uniform distribution and dispersion of the nanoparticles.Subsequently, individual tiny droplets of the diluted suspension were deposited onto a 300-mesh copper grid coated with holey carbon film. Careful removal of excess liquid was achieved using filter paper, optimizing the deposition process for TEM analysis. The as-obtained specimens were then subjected to a vacuum drying process, further enhancing the stability and preservation of the nanoparticles. The morphological analysis was conducted using an 80 kV JEOL JEM-2100 Analytical Transmission Electron Microscope, providing high-resolution imaging of the nanoparticle samples. This cutting-edge instrument allowed for detailed visualization of the nanoparticles at the nanoscale, enabling the observation of their size, shape, and overall structural integrity.

2.11 Scanning electron microscopy (SEM):

The nanostructures of PS-NPs, CTB-PS-NPs, CS-NPs, CTB-CS-NPs, PS-CS-NPs, and CTB-PS-CS-NPs were examined using ZEISS Sigma and GeminiSEM at 20 kV. Starch nanoparticles were affixed to SEM stubs with cellophane tape, and gold-palladium-coated stubs were used for morphological analysis. Digital image analysis indicated starch granules transformed into spherical particles (160-210 nm). This SEM study offers crucial insights into the morphology and size distribution of the nanoparticles, vital for their applications in drug delivery and biomedicine.

2.12 Dynamic light scattering (DLS) for Particle size analysis and Zeta potential:

The hydrodynamic diameters of PS-NPs, CTB-PS-NPs, CS-NPs, CTB-CS-NPs, PS-CS-NPs, and CTB-PS-CS-NPs was determined using a Delsa Nano C photon correlation spectroscopy (PCS) (Beckman Coulter, USA). Which supports the Non-Invasive Back Scatter (NIBS) of Dynamic Light Scattering (DLS) principle. Static Light Scattering at 173° is possible with this instrument. ZETASIZER NANO ZS included a temperature-controlled cell holder and a He-Ne laser (4 mW; 633 nm). The samples were analysed at 25°C with 21 CFR Part 11 compliant software3 after diluting with deionized water. In optically homogeneous quartz cylinder cuvettes, the average size of the nanoparticles and the polydispersity index (PDI) were measured at 25°C with a 90° angle detection. Each 0.5µL sample was dispersed in 2 mL of deionized water and measured three times to measure average size and PDI. Using a Malvern ZS90-ZETASIZER NANO ZS instrument (Malvern Instruments Ltd., UK,) the zeta potential of the nanoparticles was measured. By putting an electric field across the polymeric nanoparticle's dispersion, we may calculate its zeta potential. When a surface charge is present in the outer surface of nano-dispersion, particles having that potential will move toward the electrode with the opposite charge at a pace that is directly proportional to the strength of the zeta potential[16].

2.13 Fourier transform infrared spectroscopy (FT-IR):

The Capecitabine (CTB), PS-NPs, CTB-PS-NPs, CS-NPs, CTB-CS-NPs, PS-CS-NPs, and CTB-PS-CS-NPs infrared spectra were recorded in the range of 4000-500 cm^{-1} at a resolution of 4 cm^{-1} using a Nicolet iS50R Research FTIR Spectrometer (Thermo Fisher Scientific, USA). The OMNIC 8.3 software (Thermo Fisher Scientific, USA) was used to collect 32 repetitive scans for each spectrum[17-19].

2.14 Differential scanning calorimeter (DSC):

Using a differential scanning calorimeter (DSC1; Mettler Toledo, Schwerzenbach, Switzerland) the gelatinization limits of Capecitabine (CTB), PS-NPs, CTB-PS-NPs, CS-NPs, CTB-CS-NPs, PS-CS-NPs, and CTB-PS-CS-NPs were determined. The 5mg samples were placed into aluminium pan and 10µL milli Q water was added to make a uniform slurry while calculating the DSC thermogram. Dry nitrogen was mixed with slurry to prevent condensation. Furthermore, the hermetically sealed aluminium pan was heated at a rate of 10°C /min from 20°C to 200°C. Sample data was recorded using the STAR@ SW 9.20 data recording software. The transition temperatures, such as onset (T_o), peak (T_p), and conclusion (T_c), as well as the enthalpy of gelatinization (ΔH), were recorded for the samples during DSC analysis. The area between the thermogram and a baseline under the peak in Joules per gram of dried sample was integrated to calculate the enthalpy of gelatinization (ΔH)[20].

2.15 X-ray diffraction (XRD):

The crystalline structures of the native starch, Capecitabine (CTB) and PS-NPs, CTB-PS-NPs, CS-NPs, CTB-CS-NPs, PS-CS-NPs, CTB-PS-CS-NPs were examined by ARL EQUINOX 100 X-ray Diffractometer (Thermo Fisher Scientific, USA). The samples were stored in a sealed container in a saturated solution (1000 ml) of NaCl to standardize moisture content with Cu Kα radiation (= 1.543). Reflection angle signals of 2ɵ from 4◦to 40◦ and step length of 0.02 were recorded[21]. Relative crystallinity of samples was determined by plotting the peak's baseline on the diffractogram and calculating the area using the software spectrum viewer, according to the method described by Xiaoping Wang et al., (2022)[22]. The area above and under the curve corresponded to crystalline domains and amorphous regions, respectively. The ratio of upper area to total area was taken as the relative crystallinity: Relative crystallinity (%) = Area under the peaks/Total curve area × 100.

2.16 Thermogravimetric analysis (TGA):

The thermal properties of Capecitabine (CTB), PS-NPs, CTB-PS-NPs, CS-NPs, CTB-CS-NPs, PS-CS-NPs, and CTB-PS-CS-NPs were investigated using the TGA 2: Thermogravimetric Analyzer with the large furnace (LF) (Mettler-Toledo India Private Limited, Mumbai, India). While measuring, 5mg of each sample was placed in a platinum pan and heated at a rate of 10 C/min from 45°C to 500°C. A nitrogen gas flow of 30mL/min was used to maintain the inert nitrogen environment[23].

2.17 Surface Enhanced Raman Scattering (SERS):

An argon-ion laser was used as an excitation source for Raman spectral analysis. Using CytoSpec software wave-number region set between 2000 and 500 cm^{-1}. The laser power was kept at 8mV while it was running. To record Raman spectroscopy (WITec Alpha300+, GmbH, Ulm, Germany), a 532 nm excitation wavelength was used. Raman spectroscopy aids in the identification of different Capecitabine (CTB) encapsulated potato starch nanoparticles; additionally, Raman spectroscopy allows for the detection of the vibrational, rotational, and molecular states of the chemical composition of nanoparticles. The nanoparticles were coated on a glass slide (spread dimensions: 0.8 cm width and 1cm length) and Raman spectra were recorded while characterising CTB encapsulated potato starch nanoparticles using SERS when the spectrum from potato starch was used as a control. Each sample was run three times to see if any differences could be found[24].

2.18 Rheological estimation of starch nano-particles:

PS-NPs, CTB-PS-NPs, CS-NPs, CTB-CS-NPs, PS-CS-NPs, and CTB-PS-CS-NPs were heated to 95°C for 15 minutes in an IKA C-MAGHS7 Hot Stirrer to determine their rheological properties. After cooling, the rheology of each gel made from individual nanoparticles was measured at 25±0.1 C using a

Programmable Touch-screen Viscometer (Biuged Laboratory Instruments, China). With a delay time of 10 seconds and a shear rate of 0.1 to 100 s, the flow properties were determined. Stress sweep tests at a constant frequency of 1 Hz with a logarithmic increase in shear stress from 0.01 to 100 Pa were used to determine the viscoelastic range[25].

2.19 Antioxidant analysis:

Each 30mg sample of PS, PS-NPs, CTB-PS-NPs, CS-NPs, CTB-CS-NPs, PS-CS-NPs, and CTB-PS-CS-NPs was mixed with a 10mL solubilizing agent called dimethyl sulphoxide (DMSO) until complete dissolution obtained. Furthermore, a 300µL sample mixture dissolved in DMSO was introduced to 300µL of 0.01% 1,1-dihpenyl-2-picrylhydrazyl (DPPH) to cheek scavenging activity[26]. The final volume was adjusted to 3mL by adding 2.4mL of DMSO and, at 37°C, incubated samples for 30 minutes. The absorbance of each sample was measured at 527nm after incubation at 35°C for 25 minutes against DMSO as a control. Using the prescribed formula **(Eq.1)**, the percentage inhibition was calculated:

$$\% \text{ Inhibition} = 1 - \frac{(\text{A sample at } 527)}{(\text{B control at } 527)} \times 100 \quad \text{..... (Eq.1)}$$

2.20 Lipid peroxidation inhibition:

Aldehydes derived from lipid peroxidation play an essential role in human health and disease because they function as important signalling intermediates in modulating cellular physiological function by regulating a variety of transcription factors[27]. To measure the lipid peroxidation inhibition activity of PS-NPs, CTB-PS-NPs, CS-NPs, CTB-CS-NPs, PS-CS-NPs, and CTB-PS-CS-NPs, each 200µL samples were added into 0.4% linolenic acid, 0.4 mL of H_2O_2 (30 mM), 0.4mL of ascorbic acid (100mM) and 0.4mL of ferric nitrate (30mM). The mixture was slightly Shaked and incubated at 37°C in a water bath for 1.5 hr. After adding 2mL of TCA (trichloroacetic acid, 10% w/v) and 2.5 mL of TBA (thiobarbituric acid, 1% w/v) in the mixture, the reaction was stopped. The resultant mixture was boiled for 20 minutes in a water bath and further centrifuged at 7500 rpm for 15 minutes. The clear upper layer was collected and measured at 535nm where blank mixture was considered as control. Using **Eq.2,** the percentage inhibition was calculated

$$\% \text{ Inhibition} = [1 - \frac{(A \text{ sample at } 535)}{(A \text{ control at } 535)}] \times 100 \quad \text{..... (Eq.2)}$$

2.21 Evaluation of Capecitabine (CTB) loading in starch nanoparticles:

100 mg of Capecitabine (CTB) was dissolved into 10 mL of methanol, and the rest of the CTB-loaded CTB-PS-NPs, CTB-CS-NPs and CTB-PS-CS-NPs were prepared using the same method. The loading efficacy and loading capacity of CTB encapsulated nanoparticles were determined by recovering Capecitabine (CTB) from the CTB encapsulated nanoparticles while treating them with ultrasonication[28]. Briefly, each CTB loaded 100mg CTB-PS-NPs, CTB-CS-NPs and CTB-PS-CS-NPs were dispersed into 10mL methanol, and each mixture was ultrasonicated for 5 minutes. The amount of CTB in the nanoparticles was determined by the HPLC system (1290 Infinity II LC System, Agilent, USA), which consisted of a high-speed pump (1290 Infinity II High-Speed Pump, Agilent, USA), a wavelength detector (1290 Infinity II Diode Array Detector, Agilent, USA), and an automatic sampling system (1290 Infinity II Diode Array Detector, Agilent, USA). 2D-LC Software (Agilent, USA) was used for monitoring and interpretation. The Capecitabine (CTB) concentration was detected at a wavelength of 241nm, and RP-HPLC was accomplished using the Zorbax Eclipse Plus C18 column (4.6 ×100 mm, 3.5µ) with a mobile phase of pH4.5 Methanol: Ammonium acetate buffer (60:40) at a flow rate of 1mL/min, column temperature at 25°C, injection volume 15µL and 5 min run time. The loading efficacy and loading capacity were calculated using the following formula **(Eq.3 & Eq.4)**.

$$\text{The loading efficacy (\%)} = \frac{\text{(Total CTB added} - \text{un encapsulated CTB}}{\text{Total CTB added}} \times 100 \quad \ldots\ldots\ldots\ldots\ldots\ldots \textbf{(Eq.3)}$$

$$\text{Loading capacity (\%)} = \frac{\text{Total amount of CTB incorporated} - \text{Free amount of CTB}}{\text{CTB loaded strach nanoparticles weight}} \times 100 \quad \ldots\ldots\ldots\ldots \textbf{(Eq.4)}$$

2.22 Drug release in phosphate-buffered saline (pH 7.4):

A known concentration of CTB-loaded nanoparticles was mixed with pH 7.4 phosphate-buffered saline solution and deposited inside a dialysis bag with a molecular weight cutoff of 12,000 Da for this experiment. The dialysis bag acted as a semipermeable membrane, permitting the controlled discharge of CTB from nanoparticles while retaining the nanoparticles within. In order to monitor the release kinetics, samples of the release medium were collected at regular intervals. The collected samples were then measured for CTB concentration using High-Performance Liquid Chromatography (HPLC). This allowed researchers to construct a release profile depicting how CTB was released from the nanoparticles over time in the phosphate-buffered saline solution with a pH of 7.4 (pH 7.4). The experiment revealed important information about the drug release behaviour of CTB-loaded nanoparticles and their potential as a drug delivery system.

2.23 *In Vivo* Antitumour Activity:

Upon obtaining the requisite authorization from the Committee for the Purpose of Control and Supervision of Experiments on Animals (CPCSEA) (approval number: 14010/c/11/CPCSEA), all animal experimentation was conducted at the Deshpande Laboratory in Bhopal, India. The Helsinki Principles were adhered to throughout the course of the animal experiments. In a standard light-dark cycle, the 20-30g Balb/c albino mice were housed in plastic cages in groups of seven, with free access to food and water [29]. N, N-Dimethylhydrazine (D161608, Sigma-Aldrich, Bangalore, India) was administered intraperitoneally (IP) to male Balb/c mice for seven weeks to induce colon cancer. Male Balb/c mice were separated using randomised grouping. The male Balb/c in **Group 1** received a saline water injection intraperitoneally. To induce colon cancer in the **Group 2** male Balb/c mice, a 15 mg/IP injection of N, N-Dimethylhydrazine (DMH) was given for sixteen weeks. **Groups 3** and **Groups 4** were first given a 15 mg/IP DMH injection, followed by a daily dose of 10 mg/kg IP Capecitabine (CTB) from week 12 to week 17. The male Balb/c mice in **Groups 5, Groups 6, and Groups 7** were given 15 mg/IP DMH injections according to the above schedule, and Group wise was given lyophilized CTB-loaded CTB-PS-NPs, CTB-CS-NPs, and CTB-PS-CS-NPs daily from week 12 to week 17 intraperitoneally (IP). The lyophilized formulations were administered daily at 10:00 hr. The control group received the 10mg/kg IP Capecitabine (CTB) dose daily parallel to the dose in the **Group 3 to Group 7**.

2.24 Scarification and tumour bulb of colon dissection:

Before the mice were killed by cervical dislocation, they were given thiopental anaesthesia. Tissues from the colon and tumour bulbs from the descending colon were collected and preserved overnight in 10% formalin (CH_2O) containing a pH 7.4 phosphate buffer solution, before being implanted in paraffin wax.

2.25 Histopathological examination:

Colon tissues were fixed in formalin and then paraffined, and 4µM slices were cut and kept for further processing using a Weswox advance rotary microtome ARMT-1090A. Hematoxylin (H9627, Sigma-Aldrich, Bangalore, India) and 0.5 % (w/v) Eosin solution (Biopharm Inc, USA) were also used to stain tissues, which were then examined using a Labovision Binocular Compound Microscope with Led Illumination System. Each group sample was divided into three sections, with images captured at 100X and 400X magnification using a digital camera. For the specimens stained with Hematoxylin, histological scoring was used to determine the degree of dysplasia. Mucus cells with basal-oriented nuclei and apical localization are considered normal goblet cells with no dysplasia[30]. Hyperchromasia occurs when tissue specimens appear elongated in the microscope with hypercellularity and nuclear stratification, indicating mild dysplasia. Furthermore, tissue specimens with elongated basophilic cytoplasm, severe focal lesions with nuclear stratification, anomalies, hypercellularity, expanded vesicular and conspicuous nucleoli, loss of mucosal architecture in the crypts, focal lesions with nuclear stratification, and reduction

or elimination of the number of goblet cells are characterised as moderate dysplasia in the microscope. Aside from that, each experimental group's percentages of crypts with typical architecture and crypts with mild, moderate, or severe dysplastic alterations were calculated and average was recorded.

2.26 Western Blot Analysis:

For proper execution of western blot analysis, radioimmunoprecipitation assay buffer (RIPA buffer) was used. For the preparation of RIPA buffer, 30mM HEPES(4-(2-hydroxyethyl)-1-piperazineethanesulfonic acid), pH 7.4 150mM NaCl, 1% Nonidet P-40, 0.1% sodium dodecyl sulfate, 0.5% sodium deoxycholate is required. The isolated colon tissues were admixed with RIPA buffer containing protease & phosphatase inhibitors and further tissue homogenized for 15 minutes. The obtained Homogenates were centrifuged at 18,000 × g for 30 minutes at 4 C to remove insoluble tissues[31, 32]. The obtained supernatant was transfer to microcentrifuge tube and to determine protein concentration 5µL supernatant analysed using Bio-Rad Protein Assay Kit I with Bovine γ-globulin (BGG) standard. Further, colon tissues were isolated to homogenate and denatured with 2X Laemmli sample buffer. Further, 5µL of protein supernatant was loaded onto sodium dodecyl sulfate polyacrylamide gel (TruPAGE™ Precast Gels, Sigma Aldrich-Merck, Bangalore, India) and electrophoresis analysis were performed. During this process, in the nitrocellulose membranes (Bio-Rad, Hercules, CA, USA) the obtained protein from gels were placed and incubated for 1 hr in 5% nonfat lyophilised blocking made up of milk on the membranes. After that, the blocked membranes were washed and incubated overnight with primary antibodies specific for the targeted proteins: a rabbit recombinant polyclonal anti-cluster of differentiation 31 (CD31) antibody (RM1006) (ab281583 Abcam) at 1/1000 dilution, a mouse monoclonal antibody to VEGF165, Human (HEK 293-expressed) from Genscript Biotech Corporation (Piscataway, New Jersey, USA) at dilution 1:200 and antibody to β-actin overnight at 4°C with gentle agitation[33]. The blots were then washed and incubated with the appropriate secondary antibody, which was horseradish peroxidase (HRP) and goat anti-mouse conjugated. Then, using the ECL Advance TM Western blotting detection kit, they were enhanced chemiluminescence-detected. The ImageJ software (NIH, Bethesda, MD, USA) was used to measure the amount of immunoreactivity using densitometry

2.27 Enzyme Linked-Immunosorbent Assay for the Proangiogenic Factors:

The colon homogenates were evaluated for IL-6, TNF-α, and VEGF using the following ELISA kits: Mouse IL-6 ELISA Kit (Sigma-Aldrich), mouse TNF- ELISA kit (MaxSignal® HTS DON ELISA Kit USA), and mouse VEGF-A Mouse ELISA Kit (R&D Systems) (Thermo fisher scientific,USA). At 450 nm, the optical density of the reactions was measured[34].

2.28 Haemolysis study:

For the purpose of determining the nano formulation's quality and biocompatibility, a haemolysis study is necessary. Homolysis testing was carried out by extracting blood samples from mice using retro-orbital sinus[35]. At room temperature, 1.0 mL of blood was centrifuged for 10 minutes at 1345xg for 10 minutes. The graduated centrifuge tubes used in this experiment had previously been sterilised before being used. Scraping the plasma coating with micropipettes during centrifugation was done with these devices. Normal saline solution was used to dilute and suspend the formed erythrocyte pellets at the bottom of the graduated centrifuge tubes. The erythrocyte suspension was further diluted with 10 mL of saline water, followed by the addition of 10, 50, and 100 µg/mL of Capecitabine (CTB), CTB-loaded CTB-PS-NPs, CTB-CS-NPs and CTB-PS-CS-NPs and placebo nanoparticles (PS-NPs, CS-NPs, PS-CS-NPs) combined with 2mL of erythrocyte suspension in sterile tubes separately. In positive controlled, which fully haemolyzed erythrocytes, was rendered by dissolving 1% triton X-100 in erythrocyte solutions. The negative control test, in which erythrocytes are not haemolyzed, was made by suspending erythrocytes in regular saline solution in previously sterile Eppendorf tubes. The samples were incubated for at least 15 minutes at 37°C. Nearly 200µL samples were removed at specific pre-determined time intervals, i.e., 0.5, 1, 2, 4,5, 6,7,8, 9, and 10 hr, thus centrifuging at 1345xg for 15 minutes. A 100µL supernatant was incubated for 45 minutes at room temperature to achieve adequate haemoglobin to oxyhaemoglobin conversion. The absorbance was spectrophotometrically measured at 580 nm. The percentage of haemolysis can be determined using the following **Eq.5**

$$\% \text{ Haemolysis} = \frac{A\ sample - A\ spontaneous\ control}{A\ positive\ control} \text{ x } 100 \quad \text{..... (Eq.5)}$$

Where, the absorbance of the test sample containing the drug-loaded nanoparticles is referred to as A_{sample}. The absorbance of erythrocytes that have been previously incubated with saline water serves as $A_{spontaneous\ control}$. The absorbance of the supernatant of erythrocytes exposed to a 1% Triton X-100 solution made up of normal saline served as a positive control. The experiment was done three times and the results were expressed as mean ±SD (n=3).

2.29 Cytotoxicity assay:

To determine cellular metabolic activity, cytotoxicity, and cell viability, the MTT [(3-(4, 5-dimethylthiazol-2-yl)-2, 5-diphenyl tetrazolium bromide)] assay was used. Mosmann T. et al. (1983) discussed the MTT assay, a colorimetric assay system, for the first time[36]. The MTT assay can help researchers find cell growth inhibitors in HT-29 (91072201-DNA-5UG, Sigma-Aldrich, India) a human colorectal adenocarcinoma cell line with epithelial morphology. MTT is a pale-yellow substrate that is cleaved into a dark blue formazan product by living organisms[37]. The number of viable cells present is directly proportional to the number of MTT dissociated, which can be ascertained using a colorimetric assay. A continuous flow of 5% CO_2 was maintained at 37°C for HT-29 cell growth. Cell growth was accomplished using McCoy's 5A + 2mM Glutamine + 10% Foetal Bovine Serum FBS / FCS. The HT-29 cells were seeded

in 96-well plates, and cell viability was determined after 24 and 48 hours of incubation with different concentrations of free Capecitabine (CTB), CTB-loaded CTB-PS-NPs, CTB-CS-NPs, and CTB-PS-CS-NPs.

2.30 Cellular uptake of nanoparticles

In 12-well plates, HT-29 cells were planted at densities ranging from 13,000 to 300,000 cells/cm^2. The cells were adhered for a full day[38]. After incubating the plates at a set temperature for 1 to 4 hours, the medium in each well was removed and replaced with 1 mL of a freshly made suspension of CTB-loaded CTB-PS-NPs, CTB-CS-NPs, and CTB-PS-CS-NPs nanoparticles. Following the incubation period, the cells were washed three times with ice-cold pH 7.4 phosphate buffer solution to eliminate any nanoparticles that had not been absorbed. For further cell separation from the wells, 0.25% Trypsin, a proteolytic enzyme, was utilised. Confocal laser scanning microscopy is a cutting-edge technique for detecting carriers within cells and quantifying their uptake of nanoparticle formulations, yielding vital information about the interaction between the formulation and the target cell. After 24 hours of cultivation on confocal dishes, HT-29 cells were stained for 60 minutes with the fluorescent dye (6-Coumarin)-CTB-PS-NPs, (6-Coumarin)-CTB-CS-NPs, or (6-Coumarin)-CTB-PS-CS-NPs. The cells were washed with PBS buffer and then fixed with 4% paraformaldehyde for 20 minutes (PFA)[39]. After being cleaned, mounted, and glycerine-sealed, the cells were observed using the BC43-ultimate benchtop confocal microscope (Oxford Instruments, UK).

2.31 Cell-Growth Curve:

To achieve 90% confluence, 30,000 HT-29 cells cells/cm^2 were seeded in 6 Multiwall Plates with a diameter of 35mm. After being diluted in a 1:10 ratio with trypan blue dye, cells were counted using an RS PRO USB Digital Microscope (Noida, India). Individual CTB-PS-NPs, CTB-CS-NPs, and CTB-PS-CS-NPs were tested at 5, 25, and 75 µg/mL concentrations for 4, 24, and 48 hours, with measurements taken at each time interval. The mean and standard divisions of each experiment were recorded three times[40, 41].

2.32 Crystal Violet Assay:

Cells that are stuck to cell culture plates are stained with the Crystal Violet and further assay was performed[42]. It needs the dead cells that are stuck to the cell culture plates to move away[43]. Washing gets rid of dead and loose cells during the test[44]. Crystal violet is used to colour the connected cells that are still alive[45]. After a 6-hour treatment with different concentrations of Capecitabine (CTB) and CTB-PS-NPs, CTB-CS-NPs, and CTB-PS-CS-NPs, the violet crystal test was used to count how many cells stuck to the plate. Crystal violet is a dye that dissolves in water and works best on DNA with a neutral pH. After the cells were treated, they were washed, dried, and stained with crystal violet-methanol. After a thorough cleaning, acetic acid was added and a reading was taken at 595 nm with a spectrophotometer. Cells that

were treated were given a score based on how much they could live, and the score for the control cells was set to 100%. Each data point was done four times, and there were five different experiments.

2.33 Wound-healing assay:

A wound healing assay is a method used in the laboratory to study how cells move and interact to each other[46]. This is also called a "scratch assay" because it is done by scratching a single layer of cells and taking pictures of them at regular intervals with a time-lapse microscope[47]. It is since cells growing in a single layer move to re-connect with other cells after an artificial wound is made. In the wound-healing assay, HT-29 cells were starved for 24 hours in a medium without serum. They were then put on six-well plates with 10^6 cells in each well, where they grew until they were all the same size. Damage was done to cell monolayers by scratching them with the tip of a pipette along the width of the well[48]. They were then washed twice with serum-free medium and put in an incubator with different concentrations of Capecitabine (CTB), CTB-PS-NPs, CTB-CS-NPs, and CTB-PS-CS-NPs. For this test, concentrations of Capecitabine (CTB) were used that did not kill cells. To observe how cells travelled inside the wound, five fields of each scratch were taken in the T0 and 24hr time frames. The wound's shrinkage after 24 hours was measured and compared to T0, which was set at 100%, to determine the test's endpoint. The ImageJ software was used to determine how well the wound had healed. In the Boyden chamber invasion assay (BD Biosciences, San Jose, CA), 2×10^3 cells were placed on the apical side of 50µg/ml Matrigel-coated filters (8.2-mm diameter and 0.5-m pore size; Neuro Probe, Inc.; BIOMAP snc, Milan, Italy) in serum-free medium with or without increasing concentrations of Capecitabine (CTB) and CTB-PS-NPs, CTB-CS-NPs 10ng/mL of VEGF was put in the basolateral chamber as a chemoattractant for HT-29 and FCS 20%cancer cells. After 6 hours, the cells on the top were taken off with Q-tips. Crystal violet was used to stain the cells on the bottom of the filter, and an inverted microscope was used to count all the fields.

In Anbazhagan Sathiyaseelan et al.'s (2022)[49] study, bimetallic silver-platinum (AgPt) nanoparticles and chitosan-fabricated cotton gauze were prepared, which were found to have excellent healing properties and were tested through scratch assay.

2.34 Tube Forming Assay:

Finding the genes and pathways involved in angiogenesis can be done quickly and quantitatively using the tube formation assay[50]. When exposed to angiogenic signals, endothelial cells continue to divide and migrate at a high rate. The tube formation assay is a fast and accurate way to find out which genes or pathways are needed to make new blood vessels[51]. The assay checks how well endothelial cells can make structures that look like capillaries when they are plated at sub confluent densities and given the right support from the extracellular matrix. Moderate drug concentrations were used for the tube formation assay. HT-29 cells were put in 48-well plates that were coated with 75µL of growth factor-reduced Matrigel, with or without increasing concentrations of Capecitabine (CTB), CTB-PS-NPs, CTB-CS-

NPs, and CTB-PS-CS-NPs. After HT-29 cells were grown in a dish for 6 hours, an inverted microscope and a digital camera were used to look at the shape of the structures that looked like capillaries. Image-Pro Plus Software for microimaging, version 5.0, by Media Cybernetics, Bethesda, MD, USA, was used as a system for taking pictures.

2.35 Reactive Oxygen Species (ROS) Assay:

Following a previously published protocol, we test the ROS generating ability of Capecitabine (CTB), CTB-PS-NPs, CTB-CS-NPs, and CTB-PS-CS-NPs on HT-29 cells[52].

2.36 Apoptosis induced by CTB-loaded CTB-PS-NPs, CTB-CS-NPs, and CTB-PS-CS-NPs nanoparticles:

CTB-loaded CTB-PS-NPs, CTB-CS-NPs, and CTB-PS-CS-NPs nanoparticles were tested using the Annexin V method to see if they could cause apoptosis. HT-29 cells were seeded in flasks and then incubated for 24 hours at 37°C with CTB-loaded CTB-PS-NPs, CTB-CS-NPs, and CTB-PS-CS-NPs nanoparticles. The cell supernatant was washed three times with a pH 7.4 phosphate buffer solution. Annexin V-FITC was used to incubate washed cells for another 20 minutes at room temperature in a dark environment. The samples were analysed using a ZE5 cell flow cytometer analyser (Bio-Rad, USA) as described previously[53, 54].

3 Results

3.1 Transmission electron microscopy (TEM):

Transmission electron microscopy has been shown to be a useful tool for delivering information about how nanoparticles are uptake, biodistribution, and how they connect to the parts of cells and tissues. Transmission electron microscopy (TEM) can be used to look at the shape of nanoparticles with or without Capecitabine (CTB) coating. Due to the encapsulation of chitosan (CS) over potato starch (PS) encapsulated Capecitabine (CTB) polymeric nanoparticles, the size of PS-NPs to CTB-PS-CS-NPs grew by a massive proportion. TEM was used to measure the nanoparticles. The samples were kept in a copper grid with 300-mesh holes. The materials need to be dried before being used in a TEM for nanoparticle quantification **(Fig.2(a-f))**. Additionally, it was discovered through TEM investigation that nanoparticles have a somewhat hemispherical form. In dehydrated circumstances, the nanoparticles were discovered to be slightly agglomerated even though they effectively encapsulate the CTB due to internal gelation with potato starch and chitosan. One of the most recent studies by Neda Farnad et al., (2023)[55] depicted that potato starch can be conjugated with silver (Ag) nanoparticles to encapsulate riboflavin (Rf). The TEM results of the AgNPs/Rf/Starch nano capsules were found to be much similar with particles size

obtained from DLS method. In similar fashion, particles size of nanoparticles obtained from DSL and TEM results was found to be almost identical.

3.2 Scanning electron microscopy:

Advances in scanning electron microscopy (SEM) have made it possible to image single nanoparticles (NPs) with sizes well below 1000 nm. In order to understand the morphological differences between PS-NPs, CTB-PS-NPs, CS-NPs, CTB-CS-NPs, PS-CS-NPs, and CTB-PS-CS-NPs nanoparticles, SEM photomicrography study was taken into consideration. It was noted that the formulations were smooth, spherical, and uniform. In the presence of electrical bombardment, the nanoparticles were seen to be somewhat shrunken. This behavior may be a result of thermal fluctuation, which causes liquids inside the nanoparticles to evaporate. There was discovered to be a correlation between the findings from SEM and the particle size results from the Delsa Nano C. Drug-loaded nanocarriers' structures were discovered to be very different from what was anticipated when Field-Emission Scanning Electron Microscopy (FESEM) was used to photograph the particles **(Fig.2(g-i))**. The polymer matrix's spaces could be used by FESEM to observe the water phase that was present there. The particles' sizes gradually grow larger when PS and CS are used together. Our SEM results for nanoparticles are inconsistent with the size of the particles as determined by the Delsa Nano C photon correlation spectroscopy (PCS). Nanoparticles made of potato starch and coated in cinnamon oil were created by Yanli Guo et al. (2022)[56]. SEM analysis revealed that particles had many cracks and were agglomerated because of gelatinization of nanoparticles and leaching of amylose molecule from starch granules. The -OH group on starch, which can form hydrogen bond association with carbonyl and carboxyl groups, may explain the smoothness of the particle surfaces. The presence of amylose, amylopectin, and amylose in potato starch and poly(D-glucosamine) in chitosan led to a smooth but agglomerated and gelatinized formulation in our final formulation.

3.3 Particle size and zeta potential measurement:

Capecitabine (CTB) loaded potato starch (PS) and chitosan (CS) loaded nanoparticles were evolved to increase colon cancer activity to enhances targeting potential. The resultant size of the Potato Starch encapsulated polymeric nanoparticles (PS-NPs) was found to be 171±17.78 nm where else, final formulation (CTB-PS-CS-NPs) has particle size of 245±10.45 nm **(Fig.2(m-r))**. For all the formulations (PS-NPs, CTB-PS-NPs, CS-NPs, CTB-CS-NPs, PS-CS-NPs, and CTB-PS-CS-NPs) the PDI was found to be in the range of 0.18 to 0.23; which considered to be acceptable and indicating the development of homogenous polymeric nano dispersion of potato starch (PS) and chitosan (CS). The particle size of CTB-PS-CS-NPs is due to chemical and physical conjugation of potato starch (PS) and chitosan (CS) over nanoparticles surface. According to the **Fig.2(s-x)** the potential of all the formulations was found to be cationic in nature; which might be due to the presence of Cetrimonium bromide and chitosan within the nanoparticles. The amino group in chitosan has a pKa value of 6.5, thus chitosan is positively charged. On the other hand, Cetrimide or alkyl trimethylammonium bromide is a quaternary ammonium salt,

therefore the CTB-PS-CS-NPs was found to be cationic in nature. It was discovered that the zeta potential of the polymeric nanoparticles ranged from 7.3±1.09 mV to 30.3±8.09 mV mV for PS-NPs to CTB-PS-CS-NPs, indicating that the cationic nature of the nanoparticles increases as the amount of CS, PS, and cetrimonium bromide coating increases on the nanoparticles surface **(Table1)**. Particle size and zeta potential of iron and zinc nano encapsulates produced by Shivani Kaul et al. (2022)[57] based on potato starch were 340.9 nm and 354.5 nm; 0.372mV and 11.40 mV, respectively. Our formulation was determined to be more stable than the referenced study since nearly all of the formulations had a particle size of less than 200 nm and the final formulation had a zeta potential of 30.3±8.09 mV.

3.4 Fourier transform infrared spectroscopy (FT-IR):

The FTIR spectra of the drug Capecitabine (CTB) showed characteristic peaks at 3330 cm^{-1}, indicating the presence of primary amides R-CO-NHR in the structure, and at 2834 cm^{-1}, indicating the presence of carboxylic acid dimer O-H stretch. As far as the FTIR spectra of PS-NPs is concerned, the characteristic peak was observed at 3418 cm^{-1} and at 2889 cm^{-1}, indicating the presence of alcoholic O-H stretch and C-H stretch. Similarly, at 3435 cm^{-1}, 3458 cm^{-1}, 3435 cm^{-1}, 3458 cm^{-1}, 3443 cm^{-1}, the rest of the nanoparticles (CTB-PS-NPs, CS-NPs, CTB-CS-NPs, PS-CS-NPs, CTB-PS-CS-NPs) exhibited the characteristic H-H stretch of amide (R-CO-NH-R).Due to the successful covalent bond between chitosan (CS) and potato starch (PS) within the nanoparticles, the FTIR spectra of CTB-PS-CS-NPs exhibit a narrow N-H starch peak at 3443 cm^{-1}. However, the N-H peaks in the FTIR spectra of all nanoparticles, including placebo, are nearly identical at 1630 cm^{-1}. In addition, FTIR spectra of CTB-PS-CS-NPs indicated PS and CS successfully conjugated on the polymeric nanoparticles' outer surface, while the drug's integrity was not compromised. There was discovered to be no chemical interaction between the polymer and the drug. The FTIR spectra of the final lyophilized CTB-PS-CS-NPs formulation revealed that the medication remains in salt form **(Fig.3(a))**. In their FT-IR investigation of prepared resistant starch nanoparticles, Xiaoxia Yan et al. (2022)[58] detected an OH stretching vibration at 3400 cm^{-1}. When compared to native starch, nanoparticles' low wave number indicates that the hydrogen bond between starch molecular chains has strengthened. The C-O group's stretching vibration in the C-O-H bond is responsible for the 1200 cm^{-1} absorption peak. The similar results from our investigation validate the FTIR results we obtained.

3.5 Differential scanning calorimeter (DSC):

Differential scanning calorimetry (DSC) study is required to comprehend the melting point of drug, drug-polymer interaction, and thermal behaviour of drug-encapsulated polymeric nanoparticles. **Fig. 3(b)** displays the DSC thermograms of PS-NPs, CTB-PS-NPs, CS-NPs, CTB-CS-NPs, PS-CS-NPs, and CTB-PS-CS-NPs. The Capecitabine (CTB) DSC curve demonstrates an endothermic melting peak at 78.34 C. Capecitabine (CTB)-encapsulated polymeric nanoparticles did not interact with polymers, showing no drug-polymer interaction. The endothermic peak of chitosan (CS) was however changed to 67.5°C. This

may be due to the encapsulation of Capecitabine (CTB) within CS nanoparticles (CTB-CS-NPs). The potato starch (PS) and chitosan (CS) encapsulated Capecitabine (CTB) nanoparticles (CTB-PS-CS-NPs) exhibited a minor endothermic peak at 81.2 C, whereas the Capecitabine (CTB) characteristic peak disappeared, which can be attributed to the drug's ability to be molecularly dispersed into the polymer matrix and the complete encapsulation of CTB within the nanoparticles. The DSC analysis also indicated that both polymers (CS and PS) are compatible with the drug (CTB), which increases the likelihood of drug entrapment within the polymer in polymeric nanoparticles. To achieve stability, it is necessary to verify compatibility between the drug and the polymer, which can be proven by DSC followed by XRD tests.

During DSC analysis, Daniel Caicedo Chacon et al. (2020) saw a number of peaks that were caused by the melting of ice crystals in potato starch (PS) nanoparticles. But the DSC curves of composite PS-based nanoparticles showed only an endothermic peak that was linked to the melting of ice crystals. Also, this thermal event was seen to happen at higher temperatures in nanoparticles made from PS than in PS alone. This is likely because water molecules and nanoparticles interact through hydrogen bonds. It is obvious from **Fig. 3b** that our DSC values correspond to the discussed study.

3.6 X-Ray diffraction analysis:

Since larger crystals imply a more crystalline structure when measured at a value in the 2Θ range, the size of the crystal is the primary factor in determining an XRD peak. Diffraction peaks for the XRD study depicted in **Fig.3c** for Capecitabine (CTB) and PS-NPs, CTB-PS-NPs, CS-NPs, CTB-CS-NPs, PS-CS-NPs, and CTB-PS-CS-NPs are displayed. The molecular crystalline form of the drug was evident in this study when pure Capecitabine (CTB) displayed sharp diffraction angles (2Θ) peaks at 12.42°, 15.03°, and 16.26°. In any of the polymeric nanoparticles' XRD patterns, there were no distinct peaks to be seen. The typical peaks disappeared after CS and PS conjugation over CTB-PS-CS-NPs, and a partial shift was seen at 14.25°, indicating that the material had changed from being more crystalline to being more amorphous. The impact of the nanoparticles dissolving in water increases because they are amorphous, which ultimately activates the diffusion mechanism in polymeric nanoparticles. The formation of a polymeric complex along with the change from crystalline to amorphous form was further supported by the diffractograms of CTB-PS-CS-NPs. The physicochemical qualities of foods made from potato starch were assessed by Yufang Guan et al., (2022)[59]. As the crystallinity of PS is reduced during processing, amorphous starch is generated, which is reflected by peaks in the XRD pattern at 17.0 2θ angles. From our current research, we can say that the PS-CS-coated nanoparticles changed into an amorphous form. This is in line with research that has already been done and published.

3.7 TGA Analysis:

TGA facilitates in the comprehension of thermal phenomena brought on by heating nanomaterials and polymer composites at a set rate and temperature. The mass of the samples is analysed in a

thermogravimetric analysis (TGA) as a function of temperature and time. Thermogravimetric analysis (TGA) is an analytical technique that evaluates the weight change that occurs as a sample is heated continuously in order to determine the percentage of volatile components and the thermal stability of a material. Thermogravimetric analysis can be used to determine how much coating is present on the surface of a nanoparticle. The sample's residual metal concentration can also be calculated using TGA tests carried out in a neutral environment. TGA can be used to determine the melting points of nanoparticles as well as how stable they are under various temperature conditions. It is confirmed by the TGA thermogram that pure Capecitabine (CTB) breaks down at a temperature of 150.21°C. In the formulations CTB-PS-NPs, CTB-CS-NPs, and CTB-PS-CS-NPs, the decomposition peak of capecitabine (CTB) did not change significantly. The change in the melting enthalpy of Capecitabine (CTB) may be brought on by the fact that it is encapsulated in polymers. It is possible that adequate CTB encapsulation in the presence of potato starch (PS) and chitosan (CS) caused the absence of the CTB melting enthalpy peak in CTB-PS-NPs, CTB-CS-NPs, and CTB-PS-CS-NPs. A drug that has been encapsulated by polymers, i.e., PS and CS may therefore have greater temperature stability. According to the TGA, the weight loss pattern is followed by almost all the CTB encapsulated nanoparticles (CTB-PS-NPs, CTB-CS-NPs, and CTB-PS-CS-NPs). After thermal decomposition was complete, all the polymeric nanoparticles burned completely with no leftover material **(Fig.3d)**.

Nano titanium was embedded in a starch film that was prepared by Kshirod K. Dash et al. (2019)[60]. TGA analysis of the pure starch-pectin film shows a single, sloppy weight-loss trend, indicating the film's high thermal stability. Thermogravimetric analysis (TGA) curves show three step losses for both pure starch-pectin films and films incorporating 2% and 4% nano-TiO2. The results of the research mentioned above were correlated with the outcomes of our work

3.8 Surface Enhanced Raman Scattering (SERS):

The Raman scattering of drug and polymeric nanoparticles is shown in **Fig. 3e**. The peak counts and locations of all the polymeric nanoparticles, as well as the averaged Raman spectra. It was discovered that PS-NPs, CTB-PS-NPs, CS-NPs, CTB-CS-NPs, and CTB-PS-CS-NPs were all very similar to one another. However, there are some intensity differences between polymeric nanoparticles and capecitabine (CTB). At 310 cm^{-1} for CTB and at 200 cm^{-1} for all the polymeric nanoparticles, the Raman signal was markedly improved. Nearly all the polymeric nanoparticles exhibit Raman bands at 56.34 cm^{-1} with strong scattering intensities. It is challenging to determine the exact location of capecitabine (CTB) adsorption on the surface of the polymeric nanoparticles because a comparison of the molecule's SERS and Raman spectra reveals only minor shifts of these modes. Capecitabine (CTB) and prepared polymeric nanoparticles, such as PS-NPs, CTB-PS-NPs, CS-NPs, and CTB-PS-CS-NPs, do not appear to interact strongly, according to the results of Raman spectra. The central C-O-C bonding of starch, nitrogen atoms from chitosan, and electrons in the pyrimidine ring of capecitabine (CTB), on the other hand, would be the possible interaction sites, according to the strong enhancements seen for all groups of modes previously

mentioned. The magnitude of the SERS response appears to have been greatest for the CTB-PS-CS-NPs, intermediate for the CS-NPs, and lower for the CTB-CS-NPs, according to **Fig.3e**.

3.9 Rheological estimation of starch nano-particles:

In **Fig.2f,** the results for the rheological properties of native potato starch and starch-loaded nanoparticles are displayed. The angular frequency (s−1) was plotted against potato starch and nanoparticles of potato starch (PS). The viscosity of starch-embedded nanoparticles (CTB-PS-CS-NPs, PS-CS-NPs, CTB-PS-NPs, and PS-NPs) was significantly greater than that of potato starch. This indicates that suspensions of starch nanoparticles are more elastic than native starch. The graph in **Fig.3f** demonstrates that starch nanoparticle suspensions are more viscous than starch suspensions containing native starch. However, as shear rate increases, viscosity decreases gradually, indicating that the fluid becomes less viscous. Several studies have also demonstrated that suspensions of starch nanoparticles are more viscous than pure starch. The flow of starch is affected by the shape, size, and distribution of the granules, as well as the amount of amylose and how the granules interact with one another. According to the findings of our study, a nanoscale reduction in the size of starch increases its viscosity. Mudasir Ahmad et al. (2020)[61] used mild alkali hydrolysis to turn starch into nanoparticles. Rheological measurements showed that starch nanoparticle suspensions were thicker than starch suspensions made with native starch. The rheological properties of starch are affected by the amount of amylose and how the granules interact with each other, as well as the shape, size, and distribution of the granules. Our research shows that reducing the size of starch to the nano level makes it thicker, which were nearly identical to those of this study.

3.10 Antioxidant analysis:

DPPH (2,2-diphenyl-1-picryl-hydrazyl-hydrate) scavenging activity of potato starch (PS), PS-NPs, CTB-PS-NPs, CS-NPs, CTB-CS-NPs, PS-CS-NPs, and CTB-PS-CS-NPs are shown in **Fig.4a**. DPPH radical scavenging potential was reported as: 20.62±3.67 %, 36.78±3.56%, 34.78±3.68%,26.89±3.72%,27.67±2.67%,34.67±3.27%, 35.78±3.56% for potato starch (PS), PS-NPs, CTB-PS-NPs, CS-NPs, CTB-CS-NPs, PS-CS-NPs, and CTB-PS-CS-NPs respectively. Due to the nanonization of starch, the antioxidant activity of starch was exponentially increased while nanoparticles and starch (15mg/mL) were dissolved in DMSO. Due to ultrasonication and alkali treatment, the DPPH activity increased. During the development of nanoparticles, the use of carbodiimide coupling reaction, ultrasonication, and alkali hydrolysis significantly enhance the superoxide anion radical scavenging capacity and chelating iron ion ability. The hydrogen bonding capacity of the polysaccharide enhances due to the introduction of the substitutional sulfate group. Recent studies also concluded that the lower molecular weight and monosaccharide composition could contribute to the antioxidant activity of starch and polysaccharide. Due to the formation of nanocomposite in our study, the molecular weight of the formulation would automatically decrease, which leads to enhance antioxidant activity. Moreover,

according to recent studies, it can be identified that ultrasonic treatment while developing starch nanoparticles could reduce the starch solution's molecular weight and viscosity. Numerous studies have found that the starch from some sources, which contains flavonoids, may have significant superoxide radical scavenging activity when fabricated with other ingredients, such as chitosan. The Superoxide anions have a substantial impact on oxidative damage in proteins' DNA. The Lipid peroxidation was reported in the succeeding inclination: potato starch-PS (20.62±4.67%), PS-NPs (46.78±7.56%), CTB-PS-NPs (48.78±4.68%), CS-NPs (30.56±4.72%), CTB-CS-NPs (32.67±6.67%), PS-CS-NPs (52.67±6.27%), and CTB-PS-CS-NPs (55.78±7.56%) **(Fig.4b)**. The results obtained were statistically significant ($P<0.05$). The PS, CS-NPs, and CTB-CS-NPs partially inhibited lipid peroxidation. While PS-NPs, CTB-PS-NPs, PS-CS-NPs, and CTB-PS-CS-NPs demonstrated more significant lipid peroxidation inhibition.Hawthorn flavonoids had evident scavenging activity against DPPH, which was discovered by Xin Huang et al. (2022)[62] when investigating the antioxidant potential of starch digestion of flavonoids from Crataegus pinnatifida. In a similar fashion, our prepared chitosan and potato starch nanoparticles also show excellent scavenging activity against DPPH.

3.11 Evaluation of Capecitabine (CTB) loading in starch nanoparticles:

Capecitabine (CTB) was encapsulated in nanoparticles of potato starch to facilitate its uniform dispersion in aqueous solution and thus accelerate its diffusion and dissolution. The drug-loading capacity of CTB-PS-NPs, CTB-CS-NPs, and CTB-PS-CS-NPs was gradually enhanced as the drug concentration increased. As the drug concentration increased, the amount of unutilized drug increased, resulting in a decline in the loading efficiency of the particles. CTB-PS-CS-NPs had the highest loading capacity (65.78±2.34%) at a drug concentration of 10 mg/mL. It was determined from **Fig.4c** that fabrication of chitosan over Capecitabine (CTB) loaded potato starch nanoparticles would increase both drug loading capacity (LC) and drug loading efficacy (LE) in comparison to CTB-PS-NPs and CTB-CS-NPs **(Table 1)**. This may be due to the combination of biopolymers such as chitosan and starch, a biodegradable and thermoplastic polymer, while encapsulating Capecitabine (CTB). To create polymeric micelles of capecitabine, Hossein Ameli et al. (2022) [63]used beta-cyclodextrin. The entrapment efficiency of 13 batches of nanoformulated methanolic extracts for drugs ranged from 39.25% to 73.00% when seen at 240 nm. In a similar fashion, our drug highest drug loading capacity was found to 59.34±8.21%, which indicates our finds coincides with already published research on capecitabine.

3.12 Drug release in phosphate-buffered saline (pH 7.4):

As depicted in **Fig.4d**, capecitabine (CTB) was completely released 5 hours after dialysis initiation. After 5 hours of initial burst releases, it was discovered that the CTB release from nanoparticles was sustained. Initial burst effects may have been caused by the presence of a drug surrounding the nanoparticle's outer surface that was not encapsulated. Dissolution of Capecitabine (CTB)-loaded nanoparticles (CTB-PS-

NPs, CTB-CS-NPs, and CTB-PS-CS-NPs) occurred in the rapid release phase during the first 20hours, and the cumulative release rate was greater than that of the original drug. With the gradual release of drugs from the surface of the nanoparticles containing Capecitabine (CTB), the rate of CTB release from within the particles slowed **(Table 1)**. Consequently, the release rate of the CTB-loaded nanoparticles became gradually slower than that of the original drug, and the cumulative release rate gradually approached that of the original drug. In addition, it was recognised that the composition of polymers and their fabrication have a substantial effect on drug release patterns. The rapid release of CTB from nanoparticle surfaces up to 5 hours (100.56±3.02%) was due to the presence of free, unencapsulated crystallised drug. The cumulative drug release (%) of CTB-PS-NPs, CTB-CS-NPs, and CTB-PS-CS-NPs was 100.178±5.78% at 100hr, 100.45±5.88% at 120hr, and 100.23±6.54% after 140 hours. Both potato starch (PS) and chitosan (CS) nanoparticles had a slow release, which could be explained by the 800-ppm phosphate bound to the starch; this increases the viscosity and gives the solution a slightly anionic character, a low gelatinization temperature of about 60°C (140°F), and a high swelling power of starch. Chitosan, on the other hand, is a linear polysaccharide made up of varying amounts of (β1→4) linked N-acetyl-2 amino-2-deoxy-D-glucose (glucosamine, GlcN) and 2-amino-2-deoxy-D-glucose (N-acetyl-glucosamine, GlcNAc) residues. After 20^{th} hour of drug release, CTB-PS-CS-NPs formulation behaving like a controlled-release formulation due to the unique gelling and biocompatibility characteristics of its fabricated polymers, i.e., PS &CS. Additionally, it was discovered that chitosan with a higher hydrophilicity improves nanoparticle water penetration. To obtain a sustained release profile of capecitabine, Chun-E Mo et al. (2019)[64] found that the higher the starting drug concentration, the longer the release period would be while generating polyhedral oligomeric liquid crystals of capecitabine.

Chitosan and potato starch may have been cross-linked during the production of capecitabine nanoparticles to produce a stable network that can regulate the rate of drug release. The mechanism of drug release in the nanoparticles of capecitabine may entail a mix of diffusion and erosion. Diffusion is the transfer of drug molecules through a polymeric network, whereas erosion is the disintegration of the polymeric matrix caused by the presence of water and enzymes in the biological milieu. Chitosan is a pH-sensitive polymer, which means that its solubility and swelling properties might vary depending on the pH of the surrounding environment. At a pH of 7.4, chitosan exists in a partly ionised state, which can reduce its solubility and swelling capabilities. This can result in a delay in drug release from capecitabine nanoparticles containing chitosan, which may account for the peculiar release pattern. It is essential to highlight, however, that the mechanisms of drug release in nanoparticle systems are complicated and can be influenced by a number of variables, including the composition and characteristics of the materials, the size and shape of the nanoparticles, and the drug loading and release rate.

3.13 *In vivo* antitumour activity:

Lyophilized CTB, CTB-PS-NPs, CTB-CS-NPs, and CTB-PS-CS-NPs were each injected intraperitoneally (IP) at 10 mg/kg into 20-30g Balb/c albino mice for the anticancer investigation. Standard-of-care chemotherapeutic drug for colorectal cancer (CRC) capecitabine (CTB) at 10 mg/kg intraperitoneally (IP)

significantly reduced tumour size in N, N-dimethylhydrazine (DMH)-induced tumour s in male Balb/c mice compared to the normal vehicle control. **Fig.5a** depicts a tumour ’s development throughout time. Capecitabine (CTB) therapy resulted in a 37.04% reduction in tumour size at 21 days, compared to the vehicle control group **(Fig.5b)**. The tumour size was reduced by 51.58% when the CTB-PS-NPs dose was compared to the vehicle control. Additionally, a 69.54% decrease in tumour growth was seen when the CTB-CS-NPs dose was compared to the vehicle control. However, when male Balb/c mice were administered lyophilized CTB-PS-CS-NPs (10 mg/kg IP.), the volume of tumour s shrank by 71.62% compared to the usual vehicle control group. Thus, CTB-PS-CS-NPs can be concluded to be effective against tumour s in biological systems. CTB-PS-CS-NPs injections resulted in unexpected weight loss and potent anti- tumour activity in the mice. This is promising evidence that the drug is penetrating tumour s. Thus, CTB polymeric nanoparticle systems fabricated from PS and CS offer the dual advantage of improving anticancer drug efficacy while also decreasing their greater dose-dependent toxicity.To combat human colon cancer, Mansi Upadhyay et al. (2019)[65] created microbeads with an interpenetrating polymeric network made of Locust bean gum and sodium alginate that encapsulate Capecitabine. When given to tumour-bearing mice orally, pure drug, standard, and improved formulations (415.54 mg/Kg equivalent to pure CAP) all significantly reduced relative tumour volume (RTV). The mice in the control group lost weight, whereas the mice in the standard and improved formulation groups showed no such weight loss. Our results corroborated those of previously published studies showing a significant reduction in tumour volume 21 days after the drug was administered in the appropriate formulation to Balb/c albino mice.

3.14 Histopathological Examination:

With the VT032-V Tech Microtome 6 (Object stage opening 31X26 mm) (Coimbator, India): the animal's colon was cut into pieces. The normal mucosa, submucosa, and musculosa were present in histopathological examinations of colon tissues from the saline group **(Fig.5c, d)** stained with hematoxylin and eosin-stained. In the mucosa, the epithelium was arranged in columns and exhibited features such as a smooth surface, acidophilic cytoplasm, and oval nuclei at their bases. While crypts have regular shapes with small openings, goblet cells have a flask-like shape due to their basally flattened nuclei and vacuolated cytoplasm. The entrances to crypts are typically somewhat small. The N, N-dimethylhydrazine (DMH) control group, in contrast, exhibited hyperplasia characterized by irregularly shaped mucosa and a slightly elevated appearance **(Fig. 5e, f)**. These individuals also had laminar cellular infiltration, distorted crypts with destroyed goblet cells, and an abnormally packed lining full of hyperchromatic nuclei. Mild dysplasia (grade 2) was observed in the colon tissue sections of the group given lyophilized CTB (10 mg/kg intraperitoneally (IP)), along with a higher number of goblet cells and fewer inflammatory cells **(Fig. 5g, h)**. Additionally, the crypts, mucosa, and submucosa had a nearly normal appearance after intraperitoneal administration of CTB-PS-NPs at a dose of 10 mg/kg **(Fig. 5 i, j)**. Like the previous example, a dose of 10 mg/kg intraperitoneally of CTB-CS-NPs **(Fig. 5k, l)** and CTB-PS-CS-NPs **(Fig. 5m, n)** showed a nearly normal appearance for crypts. Staining the colonic sections of the negative control group indicated few chronic inflammatory cells when seen under the microscope

(Fig.6a). In contrast, the N, N-dimethylhydrazine (DMH) group showed a positive dense inflammatory infiltrate containing lymphoid follicles **(Fig.6b)**. Capecitabine (CTB) 10 mg/kg group colonic sections **(Fig.6c)** showed moderate inflammation with lymphoid aggregate; CTB-PS-NPs 10 mg/kg group colonic sections **(Fig.6d)** showed mild inflammation with mild aggregates; CTB-CS-NPs 10 mg/kg group colonic sections **(Fig.6e)** showed very few inflammatory cells. Colonic sections from mice given 10 mg/kg of CTB-PS-CS-NPs exhibited significantly fewer inflammatory cells, a reduced number of dysplastic and hyperplastic polyps, and a reduced degree of cryptic deformation. To see how the colon specimens were graded for tumour s. Compared to the saline group, the colon cancer control group scored considerably higher for cryptic distortion. Mice administered 10 mg/kg of CTB-PS-CS-NPs showed significant gains in performance. **Fig.6(g-j)** shows that the colon cancer control group had significantly higher scores for hyperplasia, goblet cell depletion, and dysplasia compared to the saline group, while the group that received 10 mg/kg of CTB-PS-CS-NPs had significantly lower scores for all three conditions.As part of their work on a capacetabine-loaded lipid nanoparticle for colon cancer, Narendar Dudhipala et al., (2018) [66] created a rat model of colon cancer utilising 1, 2-dimethylhydrazine (DMH). It is hypothesised that promutagenic events, such as tumour development, are triggered by alkylation of locations in DNA. In a similar fashion, our cancer animal models were developed by using 1, 2-dimethylhydrazine (DMH)

3.15 Western Blot Analysis:

Fig.7a shows the triplicate results of a western blot analysis for the proteins CD31, VEGF, and β-actin. In our current research it was understood that when comparing N, N-dimethylhydrazine (DMH) mice to a control negative group, CD31 and VEGF protein expression levels are significantly higher in the DMH treated mice **(Fig.7b&c)**. Capecitabine (CTB), capecitabine potato starch nanoparticles (CTB-PS-NPs), and capecitabine chitosan nanoparticles (CTB-CS-NPs) significantly suppressed protein expression in mice compared to N, N-dimethylhydrazine (DMH)-treated mice. Mice given 10 mg/kg of capecitabine (CTB) showed a reduction in tumour size, but mice given 10 mg/kg of CTB-PS-CS-NPs showed an even greater reduction in tumour size.

3.16 Enzyme Linked-Immunosorbent Assay for the Proangiogenic Factors:

Significantly increased levels of IL-6 expression are linked to the progression of colorectal cancer (CRC) and poor patient outcomes. In CRC, IL-6 promotes tumour initiation and tumour growth by activating signal transducers and activators of transduction-3 (STAT3). On the other hand, tumour necrosis factor alpha (TNF-α) is a cytokine that promotes inflammation and is mainly produced by macrophages and tumour cells. It has been hypothesised that increased levels of tumour necrosis factor alpha (TNF-α) in colorectal cancer (CRC) tissues facilitate tumour growth, invasion, and metastasis. It is widely accepted that vascular endothelial growth factor (VEGF) is the primary angiogenic factor in cancers of the colon and other sites. Because of this, many investigations into VEGF expression in colorectal cancer patients

have been conducted, and many therapeutic agents that target the VEGF pathway have been tested in medical settings. VEGF, IL-6, TNF-α are the angiopoietins are among the most described angiogenic growth factors. When compared to the saline group, the colon cancer control group had three times more VEGF, three times more TNF-α, and three times more IL-6 (Fig.7d). When compared to mice without colon cancer, these three proangiogenic factors were much lower in mice that were given capecitabine (CTB), CTB-PS-NPs, and CTB-CS-NPs. Compared to the groups of mice that got 10 mg/kg of capecitabine (CTB), the CTB-PS-CS-NPs treatment made the tumour s in the mice shrink even more **(Fig.7d-f)**.

3.17 Evaluation of Homolysis:

Anaemia, jaundice, and other clinical disorders can result from the loss of red blood cells, or haemolysis, caused by the injection of drugs or nanoparticles. Because of this, it is crucial to determine the haemolysis potential of drugs intended for intravenous administration early in the product development process. It is critical to comprehend the effect and behaviour of Capecitabine (CTB), PS-NPs, CTB-PS-NPs, CS-NPs, CTB-CS-NPs, PS-CS-NPs, and CTB-PS-CS-NPs when administered via blood. Similar meniscal haemolysis was seen in **Fig.8(a-r)** for Capecitabine (CTB)-NPs, as well as PS-NPs, CTB-PS-NPs, CS-NPs, CTB-CS-NPs, PS-CS-NPs, and CTB-PS-CS-NPs. However, after 10 hours, the PS-NPs, CTB-PS-NPs, CS-NPs, CTB-CS-NPs, PS-CS-NPs, and CTB-PS-CS-NPs nanoparticles induced less haemolysis (1%) than free Capecitabine (CTB), indicating that the nano formulations had less toxicity than the drug. After 10 hours of treatment, the diameter of haemolysis cells was evaluated using image j and origin pro software **(Fig.8(s-a1))**, revealing a significantly increased frequency of haemolysis in Capecitabine (CTB), positive control treated blood samples. The presence of β-linked D-glucosamine & N-acetyl-D-glucosamine from chitosan and amylose & amylopectin from potato starch corona on the nanoparticle surface protects red blood cells from haemolysis caused by Capecitabine (CTB) (0.39%), PS-NPs (0,31%), CTB-PS-NPs (0.29%), CS-NPs (0.34%), CTB-CS-NPs, PS-CS-NPs (0.31%), and CTB-PS-CS-NPs (0.28%) respectively **(Fig.8a2-a10)**. During our previous work creating Gefitinib-loaded polycaprolactone nanoparticles, we discovered that polycaprolactone (PCL) is a hemocompatible polymer, but at higher doses, PCL can cause haemolysis. Like previous studies, we found that chitosan and potato starch triggered meniscal haemolysis in this setup, but conjugating PS and CS over CTB nanoparticles made them more blood-compatible. Accordingly, CTB-PS-CS-NPs may represent an excellent alternative for injectable drug administration in cancer therapy. In order to combat skin cancer, Prashant Sahu et al. (2019)[67] created 5-FU nanogels. When compared to a positive control, Final formulation showed negligible haemolysis at a range of concentrations. The final formulation showed almost no haemolysis at concentrations between 0.2 and 0.6 mg/ml. Results showed a linear relationship between nanogel concentration and haemolysis ratio, with slight haemolysis occurring at 0.8 and 1.0 mg/ml. Final formulation hemolysis ratio was 3.69, well within the biological safety range. We found less than 1% haemolysis in our final formulation, which is a significant improvement over the haemolysis investigation. Thus, the great biocompatibility of CTB-PS-CS-NPs has been established.

3.18 Cytotoxicity assay:

The therapeutic efficacy of a drug encapsulated in a nanoparticle would depend on whether the nanoparticle was taken up and absorbed by the body. Our previous studies suggest that chemotherapeutic drug delivery via polymeric nanoparticles can increase cytotoxicity. The 2,5-diphenyl-2-H-tetrazolium bromide (MTT) assay was used to check HT-29 cell viability during proliferation and in-vitro cytotoxicity studies. Cell viability (%) was measured using the MTT assay, which compared the effects of free Capecitabine (CTB) solution with the results of CTB encapsulated CTB-CS-NPs, CTB-PS-NPs, and CTB-PS-CS-NPs. Placebo, i.e., PS-NPs, CS-NPs, and PS-CS-NPs, were also tested against HT-29 cells to evaluate the in-vitro cytotoxicity of excipients. When HT-29 cells are cultured, their growth curves take on the shape of a sigmoid because they expand slowly at first, then exponentially increased during the logarithmic growth phase, and finally gradually settled at the plateau. **Fig.9 (a-d)** shows the growth condition of HT-29 cells after treatment with 75 µg/mL of pure CTB, CTB-CS-NPs, CTB-PS-NPs, and CTB-PS-CS-NPs. After 48 hours of treatment with 25 µg/mL, 50 µg/mL, and 75 µg/mL pure CTB, CTB-CS-NPs, CTB-PS-NPs, and CTB-PS-CS-NPs, the growth of HT-29 cells is shown in **Fig.9(a1-d1)**. According to the MTT assay, both free CTB and CTB-CS-NPs, CTB-PS-NPs, and CTB-PS-CS-NPs exhibit potent antitumour activity against HT-29 cell lines. **Fig.9(e-g1)** shows the HT-29 cells' viability and behaviour after being treated with the concentrations of drug and nanoparticles for 24 hours. After 48 hours, CTB-PS-CS-NPs with double corona, exhibits superior anticancer effects against HT-29 cell lines compared to free CTB (control). After 48 hours of incubation, **Fig.9(e2-g3)** shows that the cytotoxicity of the placebo, i.e., PS-NPs, CS-NPs, and PS-CS-NPs, was lower than that of the other formulations. **Table 2** shows the time-dependent shifts in the IC_{50} value of pure CTB, CTB-CS-NPs, CTB-PS-NPs, and CTB-PS-CS-NPs at 24 hours and 48 hours. A 24-hour incubation period yielded IC50 values of 23.45±0.63 µg/mL for pure CTB, 15.56±0.93 µg/mL for CTB-CS-NPs, 14.56±0.90 µg/mL for CTB-PS-NPs, and 10.10±0.22 µg/mL for CTB-PS-CS-NPs. The IC50 values decreased to 14.36±0.53 µg/mL, 8.72±1.03 µg/mL, 7.22±1.22 µg/mL, and 5.20±0.71µg/mL after 48 hours. PS-CS scaffolding may have amplified cytotoxic activity. CTB-CS-NPs, CTB-PS-NPs, and CTB-PS-CS-NPs all have a sustained release profile, which indicates that the drug must enter cells via endocytosis and be processed before it can be released into the culture medium. CTB-CS-NPs, CTB-PS-NPs, and CTB-PS-CS-NPs all increase CTB concentration gradually during incubation with HT-29 cells because of their sustained release profiles. The cytotoxicity tests in vitro showed that CTB-PS-CS-NPs inhibited cell growth more effectively than CTB-CS-NPs, CTB-PS-NPs, and free drug CTB. HT-29 cells were killed by CTB, CTB-CS-NPs, CTB-PS-NPs, and CTB-PS-CS-NPs, but in varying ways depending on the treatment duration and concentration. The better antiproliferative effect of CTB-PS-CS-NPs can be attributed to higher intracellular drug levels and better uptake efficiency. This could be because CS has an anticancer effect. In order to treat prostate cancer Shu-Ben Sun et al., (2015)[68] developed capecitabin encapsulated PLGA nanoparticles.The PLGA nanoparticles of capecitabine were evaluated against Hep G2 Cell line by MTT Assay. When PLGA NPs were tested on Hep G2 cells, they were more effective at stopping cancer than capecitabine. Our current research findings also suggested that CTB-encapsulated nanoparticles had significant in-vitro anticancer effects against HT-29 cells.

3.19 Cellular Uptake study:

The targeting of the nanoparticles can be tested by looking at how 6-coumarin conjugated CTB-CS-NPs, CTB-PS-NPs, and CTB-PS-CS-NPs are taken up by tumour necrosis factor (TNFα) and transforming growth factors (TGF α and β) positive HT-29 cancer cells. The chitosan and potato starch conjugation binds with TNFα and TGFα, β of HT-29 cells which makes easier for cells to take up 6-coumarin conjugated nanoparticles. The fluorescence inside the cells projecting in 2^{nd} and 4^{th} hours of incubation caused by the 6-Coumarin loaded nanoparticles. However, it was coming to notice that less than 5% of the fluorescence from the 6-coumarin conjugated; CTB-CS-NPs, CTB-PS-NPs, and CTB-PS-CS-NPs nanoparticles, was released during 2^{nd} and 4^{th} hours of cell culture. In other words, the released fluorescent markers' impact on the fluorescent image should not be considered. While performing cellular uptake studies, green 6-coumarin loaded CTB-CS-NPs, CTB-PS-NPs, and CTB-PS-CS-NPs nanoparticles, were found surrounding of the nucleus of the cells. This is the indication of nanoparticles internalization over HT-29 cancer cells. Based on pictures of HT-29 cancer cells, most of the 6-coumarin was attached to the Nanoparticles, and most of the fluorescence in the uptake samples came from the cellular-associated fluorescence NPs, not the fluorescence that was released into the medium. Also, other researchers have shown that the efficiency of cellular uptake goes up as the incubation time goes up. The higher uptake of CTB-CS-NPs, CTB-PS-NPs, and CTB-PS-CS-NPs nanoparticles happened through a process called fluid-phase endocytic uptake and active targeting **(Fig.10a)**. The therapeutic effects of drugs are improved by how well they are taken up by cells. The fact that the NPs were taken up by the cells shows that 6-Coumarin loaded nanoparticles has a strong targeting effect on HT-29 cells. Le Thi Minh Phuc et al. (2017)[69] studied the cellular uptake of polystyrene (PS) nanoparticles (NPs) and discovered that conjugating epidermal growth factor to nanoparticles increases cellular uptake. Therefore, PS-NPs were better absorbed by cells in the presence of EGF. Sucrose is known to inhibit clathrin-vesicle formation; therefore, most of the cellular uptake induced by EGF involved clathrin-coated vesicle endocytosis. In our current study, Chitosan conjugation over potato starch nanoparticles enhances endocytosis, and thus CTB-PS-CS-NPs was found to have higher cellular uptake.

Capecitabine-loaded Eudragit S100/poly (lacticco-glycolic acid) nanoparticles are being developed for the treatment of colon cancer. During a cellular uptake research, Sonia Pandey et al., (2017)[70] found that the optimised nanoparticles were taken up entirely by HT 29 adenocarcinoma cells in less than 2-4 hours. In a similar process, in our current work, 6-coumarin conjugated CTB-loaded polymeric nanoparticles were showing excellent uptake in HT-29 cancer cells within 4th hours of ingestion

3.20 Effect of CTB and CTB-CS-NPs, CTB-PS-NPs, and CTB-PS-CS-NPs in Inhibiting Cell Migration:

Cell migration assay is an essential part of cancer cell growth and metastasis after cytotoxic assay (cell viability assay with MTT reagents) screening in HT-29 cancer cell lines. The in vitro scratch assay

provides support for the hypothesis that anticancer drugs inhibit the spread of cancer cells. tumour angiogenesis is a constant process in cancer that promotes the growth of tumours by encouraging the development of new blood vessels. Endothelial cells must first figure out how to migrate before they can begin to form new blood vessels. Following 24 hours of treatment with CTB, CTB-CS-NPs, CTB-PS-NPs, and CTB-PS-CS-NPs in HT-29 cancer cell lines, MTT analysis was used to determine nontoxic concentrations. The migration test can make use of these concentrations. Multiple formulations were used to cultivate HT-29 cancer cells with and without. The results demonstrated that concentrations of CTB ranging from 10^{-7} to 10^{-9} M and concentrations of CTB-CS-NPs, CTB-PS-NPs, and CTB-PS-CS-NPs ranging from 10^{-10} to 10^{-12} M had no cytotoxic effect on HT-29 cancer cells. Because HT-29 cancer cells are used for all in vitro testing, the anticancer activity of CTB, CTB-CS-NPs, CTB-PS-NPs, and CTB-PS-CS-NPs is demonstrated by their ability to inhibit the migration of HT-29 cancer cells (0h and 6h). Crystal violet staining at 6 hours determined the effect of pure CTB, CTB-CS-NPs, CTB-PS-NPs, and CTB-PS-CS-NPs on HT-29 cell viability. Cells were left untreated (control) or treated for 6 hours with escalating concentrations of CTB (from 10^{-7} to 10^{-9} M), CTB-CS-NPs (10^{-10} to 10^{-12} M), CTB-PS-NPs (10^{-10} to 10^{-12} M), CTB-PS-CS-NPs (10^{-10} to 10^{-12} M). In order to compare treated cells to controls, the control cells were set at 100% and the treated cells were expressed as a percentage of viability inhibition. They represent the mean ± SD of five independent experiments with four replicates each **(Table 3)**. The scratch-wound assay is an easy and repeatable method for measuring fundamental aspects of cell migration such velocity, tenacity, and directional preference. When cells have reached confluence, a "wound" is created by scratching them with a pipette tip. Damaged cells polarise and move into the wound cavity. The scratch-wound assay results show that CTB-CS-NPs, CTB-PS-NPs, and CTB-PS-CS-NPs inhibit cell migration for at least 7 hours after treatment. Scratched wound images are taken at the 7-hour mark, following an already published protocol. It is clear that CTB-CS-NPs, CTB-PS-NPs, and CTB-PS-CS-NPs all have anticancer effects due to this. The CTB-CS-NPs, CTB-PS-NPs, and CTB-PS-CS-NPs all had the same effect on the cells as the positive control; they inhibited their motility (CTB). Using the information, we have thus far documented regarding the control group, the 0h and 7h treatment groups, and the wound area, we analyse the images using ImageJ software. When compared to the control group, the result is the ratio of the 0 h treatment group to the 7 h treatment group (fold change) **(Fig.10b&c)**. Circular RNAs (circRNAs) were hypothesized by Jiabin Du et al. (2020)[71] to have a role in colorectal cancer cell migration and invasion via regulating miR-338-3p/TYRO3. The wound healing efficiency of SW620 and HT29 cells was drastically decreased due to a downregulation of circRAE1 in the scratch tests. Our results are consistent with those of the aforementioned study, lending integrity to our investigation.

3.21 Tube forming assay:

The effect of CTB, CTB-CS-NPs, CTB-PS-NPs, and CTB-PS-CS-NPs on angiogenesis was tested using the endothelial tube formation assay, which can predict the growth of three-dimensional cell lines vessels *in vitro*. HT-29 cancer cells were placed on 24-well plates that had been coated with 50µL of growth factor-reduced Matrigel (BD Biosciences) in the absence or presence of nontoxic concentrations of CTB (from

10^{-7} to 10^{-9} M), CTB-CS-NPs (10^{-10} to 10^{-12} M), CTB-PS-NPs (10^{-10} to 10^{-12} M), and CTB-PS-CS-NPs (10^{-10} to 10^{-12} M) **(Table 2)**. After 6 hours, the cells structures were looked like a capillary. The results showed that endothelial tube formation was stopped by CTB, CTB-CS-NPs, CTB-PS-NPs, and CTB-PS-CS-NPs in a dose-dependent way **(Fig.11a)**. In **Fig.11b**, the amount of the inhibition is shown. At doses between 10^{-7} and 10^{-9} M, CTB stopped tubes from forming, but CTB-PS-CS-NPs were more effective at stopping tubes from forming at doses between 10^{-10} and 10^{-12} M.

Nausicaa Clemente et al., (2019)[72] developed Paclitaxel-Loaded Nanosponges (PTX-PNs) and tested their ability to suppress proliferation and angiogenesis in a melanoma cell model by performing an endothelial tube formation experiment. This test involves the formation of vessels in three dimensions. Twenty-four well plates were planted with HUVECs cells for the purpose of evaluating angiogenesis. According to the findings, both PTX and PTX-PNS suppressed endothelial tube formation in a dose-dependent manner. In our experiments, also we observed our final formulation as well as drug inhibits endothelial tube formation in a dose-dependent manner in HT-29 cancer cells

3.22 Reactive Oxygen Species (ROS) Determination:

The role of reactive oxygen species (ROS) in cancer cell survival and death is bidirectional. The cancer cells undergo apoptosis because of oxidative stress caused by an increase in ROS. When compared to Capecitabine (CTB) **(Fig.11c)**, HT-29 cancer cell lines treated with CTB-PS-NPs, CTB-CS-NPs, and CTB-PS-CS-NPs for 5 hours indicate higher formation of ROS (here H_2O_2) by exhibiting brilliant green coloured fluorescence **(Fig.11d)**. CTB nano formulation treatment for HT-29 cancer for 24 hours may have had comparable results. There is some ROS identified in untreated HT-29 cancer cells because their metabolism is higher than that of normal cells. Previous research has shown that silver nanoparticles, like chemotherapy medicines, can inhibit tumour growth by increasing oxidative stress. Its powerful anticancer action in the HT-29 carcinoma may be due to the ROS production by the PS and CS in CTB encapsulated nanoparticles.

Using U-87 cancer cells, Shagufta Haque et al. (2021)[73] measured the levels of reactive oxygen species (ROS) while developing silver nanoparticles for cancer therapy. Cancer cells are killed by apoptosis when the amount of ROS increases, which causes oxidative stress within the cells. After 5 hours of AgZE treatment, U-87 cells exhibit intense green fluorescence, indicating enhanced formation of reactive oxygen species (ROS; in this case, H2O2). AgZE's powerful anticancer effect in U-87 cells may be due to its ability to generate reactive oxygen species (ROS). The aforementioned research had significant similarities with our research outcomes, ultimately validating our analysis.

3.23 Apoptosis induced by CTB-loaded CTB-PS-NPs, CTB-CS-NPs, and CTB-PS-CS-NPs nanoparticles:

In our research, we studied how CTB-PS-CS-NPs affect HT-29 cancer cells. We wanted to see if these nanoparticles trigger a process called apoptosis, where damaged cells self-destruct. We prepared cell samples from treated and untreated groups and used FITC Annexin-V staining and flow cytometry to identify apoptotic cells. Results were shown in histograms and bar graphs, indicating the percentage of apoptotic cells in different groups **(Fig.12(a-b))**. Control group: No treatment, CTB-PS-NPs group: Treatment with CTB-PS-NPs, CTB-CS-NPs group: Treatment with CTB-CS-NPs, CTB group: Treatment with capecitabine directly, CTB-PS-CS-NPs group: Treatment with our specific nanoparticles (CTB-PS-CS-NPs) Statistical analysis using Student's t-test revealed a significant difference (*$p < 0.01$) in the effectiveness of CTB-PS-CS-NPs in inducing apoptosis compared to the untreated group.

Apoptosis tests were conducted on the A549 cell line by Abdelrahman Y. Sherif et al. (2022)[74] while developing the Gefitinib Nanoscale Lipid-Based formulation. Examination of apoptosis confirmed that a sophisticated physiological process had eliminated the unwelcome cells. Pure GEF treatment of A549 cells was detected in this study by Annexin V/PI double labelling. The cytotoxic action of GEF is increased at low concentrations by the addition of GEF-TPGS-NLC. Our results are consistent with those of the aforementioned study, lending credibility to our investigation.

4 Discussion

The comprehensive investigation conducted in this study elucidates the pivotal role of potato starch in the synthesis of chitosan-based nanoparticles, particularly designed for the targeted delivery of capecitabine in colon cancer treatment. The developed nanoparticles, denoted as CTB-PS-CS-NPs (Capecitabine-Potato Starch-Chitosan Nanoparticles), harnessed the stabilizing attributes of potato starch to ensure uniform size and shape during synthesis, a critical factor for efficient drug delivery. Beyond mere stabilization, potato starch significantly influenced the release profile of capecitabine, quantifiably improving the controlled release dynamics. This modification, characterized by an initial burst release followed by a prolonged phase, holds paramount importance in enhancing therapeutic efficacy while minimizing adverse effects, particularly crucial in the context of chemotherapy regimens. Chitosan, as the primary polymer and structural backbone of CTB-PS-CS-NPs, played a pivotal role throughout the fabrication process. Its positively charged surface facilitated electrostatic interactions with negatively charged capecitabine molecules, underscoring its significance in drug encapsulation. The protonation of chitosan's amino groups in an acidic solution proved instrumental in enhancing its solubility in water-based solutions, a prerequisite for successful nanoparticle formulation. The incorporation of capecitabine, coupled with the addition of the cross-linking agent tripolyphosphate polyanion (TPP), further augmented stability. TPP's role in creating potential apertures or channels within the nanoparticles has implications for improving drug loading efficiency by facilitating enhanced drug absorption. The synergistic inclusion of potato starch in the nanoparticle formulation not only strengthened stability but also increased loading capacity. The potential formation of a protective coating by potato starch around the nanoparticles reduced aggregation likelihood, contributing to improved biocompatibility. This protective coating proved instrumental in ensuring the longevity and functionality of the nanoparticles throughout their lifecycle. A comprehensive investigation of the physicochemical

properties of CTB-PS-CS-NPs was carried out through multiple analytical techniques. Fourier Transform Infrared Spectroscopy (FTIR) provided insights into the chemical composition, revealing characteristic peaks associated with primary amides and carboxylic acid dimer in capecitabine, along with peaks indicative of alcoholic O-H and C-H stretch in potato starch. Differential Scanning Calorimetry (DSC) analysis illuminated melting temperatures and drug-polymer interactions, showcasing a small endothermic peak at 81.2°C indicative of complete capecitabine encapsulation within the nanoparticles. X-Ray Diffraction (XRD) analysis contrasted the amorphous nature of the nanoparticles with the molecular crystalline form of capecitabine. Thermogravimetric Analysis (TGA) further affirmed the thermal stability of encapsulated capecitabine within the nanoparticles. The efficacy of CTB-PS-CS-NPs in cancer treatment was underscored by their performance in colon cancer mouse models. A remarkable 71.62% reduction in tumour size demonstrated the substantial therapeutic potential of these nanoparticles. Histopathological analyses provided further validation, revealing a decrease in inflammatory cells, dysplastic, and hyperplastic polyps in treated mice. Assessment of cytotoxicity and hemolysis potential indicated reduced hemolysis, emphasizing a component on the nanoparticles' surface preventing adverse effects. In vitro assays supported the anticancer potential of CTB-PS-CS-NPs, showing dose-dependent inhibition of cancer cell migration and angiogenesis.

This study signifies the significant contribution of potato starch to the formulation of chitosan nanoparticles, presenting a nanomedicine breakthrough for biocompatible cancer treatment. The distinctive synergy between potato starch and chitosan in CTB-PS-CS-NPs offers a versatile platform for further exploration in targeted drug delivery, reinforcing its potential as an effective therapeutic intervention in cancer treatment.

5 Conclusion

This study innovatively synthesized capecitabine-conjugated nanoparticles by combining potato starch and chitosan through ionotropic gelation, reinforced with mild alkali hydrolysis and ultrasonication techniques. The resulting nanoparticles demonstrated enhanced thermal stability, increased viscosity, and potent antioxidant properties, positioning them as promising candidates for advanced drug delivery. The pH-sensitive attributes of chitosan and potato starch, crucial for colon-specific drug delivery, show significant potential for regulated drug release in the colonic environment. The study shown a more amorphous structure in potato starch-chitosan nanoparticles, and particular in vitro and in vivo experiments underscored their size-dependent uptake by HT-29 cancer cells, emphasizing particles below 200 nm for optimal cellular absorption. CTB-PS-CS-NPs exhibited notable cytotoxicity in MTT assays, indicating their efficacy in cancer therapy. The research suggests an augmented bio adhesion of CTB-PS-CS-NPs, a critical factor for effective cancer drug delivery. This study not only highlights the crucial role of these nanoparticles in regulated drug distribution for cancer therapy but also emphasizes the intricate interplay between nanotechnology and tumour biology in overcoming chemo-resistance. CTB-PS-CS-NPs demonstrated superior characteristics and significant inhibition of colon cancer growth in mice, outperforming free CTB preparations by targeting angiogenesis more effectively. While these findings represent a paradigm shift in cancer nanomedicine, further research is essential to validate outcomes in

diverse animal cancer models and unlock the full potential of these innovative biocompatible nanoparticles. This research establishes a precedent in cancer nanomedicine, paving the way for novel treatment strategies and offering new possibilities in the relentless pursuit of a cure for cancer. The groundbreaking combination of potato starch and chitosan in nanoparticle formulation emerges as a transformative force, providing renewed hope in the ongoing battle against cancer.

Declarations

Ethics approval and consent to participate

This study was conducted in accordance with the Declaration of Helsinki and approved by Committee for the Purpose of Control and Supervision of Experiments on Animals (CPCSEA) (approval number: 14010/c/11/CPCSEA), all animal experimentation was conducted at the Deshpande Laboratory in Bhopal, India.

Consent for publication

Not applicable

Availability of data and material

The datasets used and/or analysed during the current study are available from the corresponding author on reasonable request.

Competing interests

Not applicable

Funding

The corresponding author acknowledges the NMIMS Deemed-to-be University Seed grant (issued on 11th July, 2022) for generously supporting this project, which facilitated the acquisition of essential chemicals and glassware

Authors' contributions

Sankha Bhattacharya; conceptualization; supervision; visualization; writing-original draft, communication to the journal. Amit Page, Prafull Shinde; writing - review & editing. Sankha Bhattacharya; validation, final approval, communication to the journal.

Acknowledgements

This initiative would not have been possible without the help and support of Dr. R.S. Gaud, Pharma Section Director, SVKM's NMIMS Deemed-to-be University, Mumbai, India. Correspondingly, the authors would like to thank DIYA LAB, Mumbai, India, for its logistical and analytical assistance throughout the

development of this project. The authors would like to thank Aakaar Biotechnologies Private Limited, Lucknow, Uttar Pradesh 226031, India for conducting entire in-vitro anticancer activity. The authors also like to express sincere regard to Deshpande Laboratories (DL) Pvt. Ltd., Bhopal, MP, India, for helping in entire in-vivo animal's studies

Authors' information (optional)

Not applicable

References

1. S. Narayana, M.G. Ahmed, B.H.J. Gowda, P.K. Shetty, A. Nasrine, M. Thriveni, N. Noushida, A. Sanjana, Recent advances in ocular drug delivery systems and targeting VEGF receptors for management of ocular angiogenesis: A comprehensive review, Future Journal of Pharmaceutical Sciences 7(1) (2021) 186.
2. R.O. Saleh, M.T.S. Al-Ouqaili, E. Ali, S. Alhajlah, A.H. Kareem, M.N. Shakir, M.Q. Alasheqi, Y.F. Mustafa, A. Alawadi, A. Alsaalamy, lncRNA-microRNA axis in cancer drug resistance: particular focus on signaling pathways, Medical Oncology 41(2) (2024) 52.
3. J. Garg, K. Pathania, S.P. Sah, S.V. Pawar, Nanostructured lipid carriers: a promising drug carrier for targeting brain tumours, Future Journal of Pharmaceutical Sciences 8(1) (2022) 25.
4. Y. Wang, M. Shi, R. Zhang, W. Zhang, Y. Liu, D. Sun, X. Wang, S. Qin, Y. Kang, Legume-potato rotation affects soil physicochemical properties, enzyme activity, and rhizosphere metabolism in continuous potato cropping, Chemical and Biological Technologies in Agriculture 10(1) (2023) 132.
5. M. Yadav, P. Goswami, K. Paritosh, M. Kumar, N. Pareek, V. Vivekanand, Seafood waste: a source for preparation of commercially employable chitin/chitosan materials, Bioresources and Bioprocessing 6(1) (2019) 8.
6. B. Palakeeti, K.V. Reddy, K.V. Gobi, P.N. Rao, J.P. Chinta, Simple and efficient method for the quantification of antiepileptic drugs in human plasma by using magnetic graphene oxide-β-cyclodextrin composite as a sorbent, Future Journal of Pharmaceutical Sciences 7(1) (2021) 93.
7. P.N. Navya, A. Kaphle, S.P. Srinivas, S.K. Bhargava, V.M. Rotello, H.K. Daima, Current trends and challenges in cancer management and therapy using designer nanomaterials, Nano Convergence 6(1) (2019) 23.
8. A. Ozaki, K. Tachibana, T. Ohtake, Correction to: Challenges and future directions in breast cancer care in Fukushima prefecture in Japan: correspondence to "A survey on the current status of clinical resources for diagnosis and treatment of breast cancer in rural hospitals of the Tohoku region in Japan", Breast Cancer 29(1) (2022) 191-191.
9. Q. Yu, Y. Zhang, Y. Tian, A. Peng, X. Cui, B. Ding, L. Yang, Y. Liu, Y. Ju, C. Gao, Correction to: Exosomal Circ_FMN2 Derived from the Serum of Colorectal Cancer Patients Promotes Cancer Progression by miR-338-3p/MSI1 Axis, Applied Biochemistry and Biotechnology (2023).

10. S. Groselli, L. Bechstein, K. Gabka, M. Ulbig, Anti-VEGF(anti-vascular endothelial growth factor)-Therapie bei Zentralvenenverschluss in der Stillzeit, Die Ophthalmologie 120(7) (2023) 751-754.
11. J. Bré, A.L. Dickson, O.J. Read, Y. Zhang, F.G. McKissock, P. Mullen, P. Tang, G.M. Zickuhr, C.M. Czekster, D.J. Harrison, The novel anti-cancer fluoropyrimidine NUC-3373 is a potent inhibitor of thymidylate synthase and an effective DNA-damaging agent, Cancer Chemotherapy and Pharmacology 91(5) (2023) 401-412.
12. H. Sultana, M.N. Aamir, A. Madni, M.u. Rehman, A. Shafiq, J.H. Shirazi, S. Hassan, Sumaira, Polymeric Nanogel for Oral Delivery of the Chemotherapeutic Agent: Fabrication and Evaluation Alongside Toxicological Studies and Histopathological Examination, AAPS PharmSciTech 24(1) (2023) 43.
13. M.H. Waliullah, T. Mu, M. Ma, Recovery of total, soluble, and insoluble dietary fiber from potato (Solanum tuberosum) residues and comparative evaluation of their structural, physicochemical, and functional properties, Journal of Food Processing and Preservation 45(7) (2021) e15650.
14. E.M.A. Hejjaji, A.M. Smith, G.A. Morris, The potential of chitosan-tripolyphosphate microparticles in the visualisation of latent fingermarks, Food Hydrocolloids 71 (2017) 290-298.
15. L. Wu, S. Lv, D. Wei, S. Zhang, S. Zhang, Z. Li, L. Liu, T. He, Structure and properties of starch/chitosan food packaging film containing ultra-low dosage GO with barrier and antibacterial, Food Hydrocolloids (2022) 108329.
16. K. Saravanakumar, B. Sriram, A. Sathiyaseelan, A.V.A. Mariadoss, X. Hu, K.-S. Han, V. Vishnupriya, D. MubarakAli, M.-H. Wang, Synthesis, characterization, and cytotoxicity of starch-encapsulated biogenic silver nanoparticle and its improved anti-bacterial activity, International Journal of Biological Macromolecules 182 (2021) 1409-1418.
17. M. Zheng, M. Pan, W. Zhang, H. Lin, S. Wu, C. Lu, S. Tang, D. Liu, J. Cai, Poly(α-l-lysine)-based nanomaterials for versatile biomedical applications: Current advances and perspectives, Bioactive Materials 6(7) (2021) 1878-1909.
18. G. Wu, Z. Gao, A. Dong, S. Yu, Calcium-induced changes in calmodulin structural dynamics and thermodynamics, International Journal of Biological Macromolecules 50(4) (2012) 1011-1017.
19. A. Dong, T. Lam, Equilibrium titrations of acid-induced unfolding–refolding and salt-induced molten globule of cytochrome c by FT-IR spectroscopy, Archives of Biochemistry and Biophysics 436(1) (2005) 154-160.
20. J.H. Ko, N.L. Forsythe, M.B. Gelb, K.M.M. Messina, U.Y. Lau, A. Bhattacharya, T. Olafsen, J.T. Lee, K.A. Kelly, H.D. Maynard, Safety and Biodistribution Profile of Poly(styrenyl acetal trehalose) and Its Granulocyte Colony Stimulating Factor Conjugate, Biomacromolecules 23(8) (2022) 3383-3395.
21. H.M. Dardeer, S.A. Abbas, G.S. El-Sayyad, M.F. Ali, Effect of titanium dioxide nanoparticles and β-cyclodextrin polymer on physicochemical, antimicrobial, and antibiofilm properties of a novel chitosan-camphor polymer, International Journal of Biological Macromolecules 219 (2022) 1062-1079.

22. X. Wang, W. Dong, P. Zhang, H. Tang, L. Zhang, T. Yang, P. Liu, H. Wang, X.D. Xiang, High-Throughput Powder Diffraction Using White X-Ray Beam and a Simulated Energy-Dispersive Array Detector, Engineering 10 (2022) 81-88.
23. M.U. Akram, N. Abbas, M. Farman, S. Manzoor, M.I. Khan, S.M. Osman, R. Luque, A. Shanableh, Tumor micro-environment sensitive release of doxorubicin through chitosan based polymeric nanoparticles: An in-vitro study, Chemosphere (2022) 137332.
24. J. Tang, Q. Zhang, J. Zhou, H. Fang, H. Yang, F. Wang, Investigation of pesticide residue removal effect of gelatinized starch using surface-enhanced Raman scattering mapping, Food Chemistry 365 (2021) 130448.
25. H. Dong, Q. Zhang, J. Gao, L. Chen, T. Vasanthan, Comparison of morphology and rheology of starch nanoparticles prepared from pulse and cereal starches by rapid antisolvent nanoprecipitation, Food Hydrocolloids 119 (2021) 106828.
26. M. Ahmad, B. Ashraf, A. Gani, A. Gani, Microencapsulation of saffron anthocyanins using β glucan and β cyclodextrin: Microcapsule characterization, release behaviour & antioxidant potential during in-vitro digestion, International Journal of Biological Macromolecules 109 (2018) 435-442.
27. H. Yong, R. Bai, F. Bi, J. Liu, Y. Qin, J. Liu, Synthesis, characterization, antioxidant and antimicrobial activities of starch aldehyde-quercetin conjugate, International Journal of Biological Macromolecules 156 (2020) 462-470.
28. G. Nandi, M.S. Hasnain, A.K. Nayak, Chapter 8 - Polysaccharide-based polyelectrolyte complex systems in drug delivery, in: A.K. Nayak, M.S. Hasnain (Eds.), Tailor-Made Polysaccharides in Drug Delivery, Academic Press2023, pp. 177-210.
29. A.K. Bakrania, B.C. Variya, L.V. Rathod, S.S. Patel, DEAE-Dextran coated paclitaxel nanoparticles act as multifunctional nano system for intranuclear delivery to triple negative breast cancer through VEGF and NOTCH1 inhibition, European Journal of Pharmaceutics and Biopharmaceutics 122 (2018) 37-48.
30. K. Ding, M. Zhou, H. Wang, S. Zhang, D.N. Metaxas, Spatially aware graph neural networks and cross-level molecular profile prediction in colon cancer histopathology: a retrospective multi-cohort study, The Lancet Digital Health 4(11) (2022) e787-e795.
31. Z. Wang, W. Li, J. Park, K.M. Gonzalez, A.J. Scott, J. Lu, Camptothesome elicits immunogenic cell death to boost colorectal cancer immune checkpoint blockade, Journal of Controlled Release 349 (2022) 929-939.
32. A.S. Doshi, S. Cantin, L.B. Prickett, D.A. Mele, M. Amiji, Systemic nano-delivery of low-dose STING agonist targeted to CD103+ dendritic cells for cancer immunotherapy, Journal of Controlled Release 345 (2022) 721-733.
33. Y. Zhai, M. Liu, T. Yang, J. Luo, C. Wei, J. Shen, X. Song, H. Ke, P. Sun, M. Guo, Y. Deng, H. Chen, Self-activated arsenic manganite nanohybrids for visible and synergistic thermo/immuno-arsenotherapy, Journal of Controlled Release 350 (2022) 761-776.

34. Z.C.T. Zaw, N. Kawashima, T. Kaneko, T. Okiji, Angiogenesis during coronal pulp regeneration using rat dental pulp cells: Neovascularization in rat molars in vivo and proangiogenic dental pulp cell-endothelial cell interactions in vitro, Journal of Dental Sciences 17(3) (2022) 1160-1168.
35. S. Bhattacharya, Fabrication and characterization of chitosan-based polymeric nanoparticles of Imatinib for colorectal cancer targeting application, International Journal of Biological Macromolecules 151 (2020) 104-115.
36. J. Zheng, B. Karmakar, A.F. El-kott, F.G. Elsaid, A.A. Shati, S. Negm, A.A. Alsayegh, G. El-Saber Batiha, Characterization and cytotoxicity and antihuman renal cell carcinoma potentials of starch capped-copper oxide nanoparticles synthesized by ultrasonic irradiation: Introducing a novel chemotherapeutic drug, Journal of Saudi Chemical Society 26(6) (2022) 101543.
37. H. Amin, S.K. Osman, A.M. Mohammed, G. Zayed, Gefitinib-loaded starch nanoparticles for battling lung cancer: Optimization by full factorial design and in vitro cytotoxicity evaluation, Saudi Pharmaceutical Journal (2022).
38. S. Shabana, H.I. Hamouda, M. Abdalla, M. Sharaf, Z. Chi, C. Liu, Multifunctional nanoparticles based on marine polysaccharides for apremilast delivery to inflammatory macrophages: Preparation, targeting ability, and uptake mechanism, International Journal of Biological Macromolecules 222 (2022) 1709-1722.
39. Z. Zhang, Y. Zhang, Y. Li, S. Jiang, F. Xu, K. Li, L. Chang, H. Gao, P. Kukic, P.L. Carmichael, M. Liddell, J. Li, Q. Zhang, Z. Lyu, S. Peng, T. Zuo, L. Tulum, P. Xu, Quantitative phosphoproteomics reveal cellular responses from caffeine, coumarin and quercetin in treated HepG2 cells, Toxicology and Applied Pharmacology 449 (2022) 116110.
40. H. Kuhn, A. Frille, M.A. Petersen, J. Oberhuber-Kurth, L. Hofmann, A. Gläser, S. Taubenheim, S. Klagges, S. Kraemer, J. Broschewitz, M. von Laffert, H. Wirtz, IGFBP3 inhibits tumor growth and invasion of lung cancer cells and is associated with improved survival in lung cancer patients, Translational Oncology 27 (2023) 101566.
41. F.R.P. Dewi, N. Shoukat, N.i.I. Alifiyah, S.P.A. Wahyuningsih, A.l. Rosyidah, M.D. Prenggono, H. Hartono, Increasing the effect of annonacin using nanodiamonds to inhibit breast cancer cells growth in rats (Rattus norvegicus)-Induced breast cancer, Heliyon 8(11) (2022) e11418.
42. M.L. Guimarães, F.A.G. da Silva, M.M. da Costa, H.P. de Oliveira, Coating of conducting polymer-silver nanoparticles for antibacterial protection of Nile tilapia skin xenografts, Synthetic Metals 287 (2022) 117055.
43. H. Cheng, Z. Jiang, C. Sun, Z. Wang, G. Han, X. Chen, T. Li, Z. Fan, F. Zhang, X. Yang, L. Lv, H. Zhang, J. Zhou, Y. Ding, Protein stabilized polymeric nanoparticles inspired relay drug delivery for tackling post-chemotherapeutic metastasis, Chemical Engineering Journal 427 (2022) 131672.
44. Abdullah, T. Hussain, S. Faisal, M. Rizwan, Saira, N. Zaman, M. Iqbal, A. Iqbal, Z. Ali, Green synthesis and characterization of copper and nickel hybrid nanomaterials: Investigation of their biological and photocatalytic potential for the removal of organic crystal violet dye, Journal of Saudi Chemical Society 26(4) (2022) 101486.

45. C.I. Amador, R.O. Stannius, H.L. Røder, M. Burmølle, High-throughput screening alternative to crystal violet biofilm assay combining fluorescence quantification and imaging, Journal of Microbiological Methods 190 (2021) 106343.
46. J. Huang, S. Wang, X. Wang, J. Zhu, Z. Wang, X. Zhang, K. Cai, J. Zhang, Combination wound healing using polymer entangled porous nanoadhesive hybrids with robust ROS scavenging and angiogenesis properties, Acta Biomaterialia 152 (2022) 171-185.
47. A. Gnerucci, P. Faraoni, E. Sereni, F. Ranaldi, Scratch assay microscopy: A reaction–diffusion equation approach for common instruments and data, Mathematical Biosciences 330 (2020) 108482.
48. W. Jin, E.T. Shah, C.J. Penington, S.W. McCue, L.K. Chopin, M.J. Simpson, Reproducibility of scratch assays is affected by the initial degree of confluence: Experiments, modelling and model selection, Journal of Theoretical Biology 390 (2016) 136-145.
49. A. Sathiyaseelan, K. Saravanakumar, M.-H. Wang, Bimetallic silver-platinum (AgPt) nanoparticles and chitosan fabricated cotton gauze for enhanced antimicrobial and wound healing applications, International Journal of Biological Macromolecules 220 (2022) 1556-1569.
50. Y. Moriiwa, N. Oyama, R. Otsuka, K. Morioka, A. Shoji, A. Yanagida, Development of a colorimetric assay for quantification of favipiravir in human serum using ferrihydrite, Talanta 252 (2023) 123827.
51. A. Laborda-Illanes, L. Sánchez-Alcoholado, D. Castellano-Castillo, S. Boutriq, I. Plaza-Andrades, L. Aranega-Martín, J. Peralta-Linero, E. Alba, A. González-González, M.I. Queipo-Ortuño, Development of in vitro and in vivo tools to evaluate the antiangiogenic potential of melatonin to neutralize the angiogenic effects of VEGF and breast cancer cells: CAM assay and 3D endothelial cell spheroids, Biomedicine & Pharmacotherapy 157 (2023) 114041.
52. L. Jin, Z. Zhu, L. Hong, Z. Qian, F. Wang, Z. Mao, ROS-responsive 18β-glycyrrhetic acid-conjugated polymeric nanoparticles mediate neuroprotection in ischemic stroke through HMGB1 inhibition and microglia polarization regulation, Bioactive Materials 19 (2023) 38-49.
53. J. Huang, Y. Ye, Y. Xiao, Q. Ren, Q. Zhou, M. Zhong, L. Jiao, L. Wu, Geniposide ameliorates glucocorticoid-induced osteoblast apoptosis by activating autophagy, Biomedicine & Pharmacotherapy 155 (2022) 113829.
54. A. Shields, A. Amcheslavsky, E. Brown, T.V. Lee, Y. Nie, T. Tanji, Y.T. Ip, A. Bergmann, Toll-9 interacts with Toll-1 to mediate a feedback loop during apoptosis-induced proliferation in Drosophila, Cell Reports 39(7) (2022) 110817.
55. N. Farnad, K. Farhadi, Introducing potato starch-ecofriendly silver nanoparticles as a novel binary system for nanoencapsulation of riboflavin, Food Chemistry 398 (2023) 133910.
56. Y. Wan, Y. Qian, Y. Wang, F. Fang, G. Wu, Prognostic value of Beclin 1, EGFR and ALK in non-squamous non-small cell lung cancer, Discover Oncology 13(1) (2022) 127.
57. S. Kaul, K. Kaur, N. Mehta, S.S. Dhaliwal, J.F. Kennedy, Characterization and optimization of spray dried iron and zinc nanoencapsules based on potato starch and maltodextrin, Carbohydrate Polymers 282 (2022) 119107.

58. X. Yan, M. Diao, Y. Yu, F. Gao, E. Wang, Z. Wang, T. Zhang, P. Zhao, Characterization of resistant starch nanoparticles prepared via debranching and nanoprecipitation, Food Chemistry 369 (2022) 130824.
59. Y. Guan, G. Zhao, S. Thaiudom, Evaluation of the physico-chemical properties of potato starch-based foods and their interactions with milk protein and soybean oil, Food Chemistry: X 16 (2022) 100495.
60. K.K. Dash, N.A. Ali, D. Das, D. Mohanta, Thorough evaluation of sweet potato starch and lemon-waste pectin based-edible films with nano-titania inclusions for food packaging applications, International Journal of Biological Macromolecules 139 (2019) 449-458.
61. M. Ahmad, A. Gani, I. Hassan, Q. Huang, H. Shabbir, Production and characterization of starch nanoparticles by mild alkali hydrolysis and ultra-sonication process, Scientific reports 10(1) (2020) 3533.
62. X. Huang, Y. Bian, T. Liu, Z. Xu, Z. Song, F. Wang, T. Li, S. Li, Antioxidant potential and in vitro inhibition of starch digestion of flavonoids from Crataegus pinnatifida, Heliyon 8(10) (2022) e11058.
63. H. Ameli, N. Alizadeh, Targeted delivery of capecitabine to colon cancer cells using nano polymeric micelles based on beta cyclodextrin, RSC Advances 12(8) (2022) 4681-4691.
64. C.-E. Mo, M.-H. Chai, L.-P. Zhang, R.-X. Ran, Y.-P. Huang, Z.-S. Liu, Floating molecularly imprinted polymers based on liquid crystalline and polyhedral oligomeric silsesquioxanes for capecitabine sustained release, International Journal of Pharmaceutics 557 (2019) 293-303.
65. M. Upadhyay, S.K.R. Adena, H. Vardhan, S.K. Yadav, B. Mishra, Locust bean gum and sodium alginate based interpenetrating polymeric network microbeads encapsulating Capecitabine: Improved pharmacokinetics, cytotoxicity &in vivo antitumor activity, Materials Science and Engineering: C 104 (2019) 109958.
66. N. Dudhipala, G. Puchchakayala, Capecitabine lipid nanoparticles for anti-colon cancer activity in 1,2-dimethylhydrazine-induced colon cancer: preparation, cytotoxic, pharmacokinetic, and pathological evaluation, Drug development and industrial pharmacy 44(10) (2018) 1572-1582.
67. P. Sahu, S.K. Kashaw, S. Sau, V. Kushwah, S. Jain, R.K. Agrawal, A.K. Iyer, pH triggered and charge attracted nanogel for simultaneous evaluation of penetration and toxicity against skin cancer: In-vitro and ex-vivo study, Int J Biol Macromol 128 (2019) 740-751.
68. S.B. Sun, P. Liu, F.M. Shao, Q.L. Miao, Formulation and evaluation of PLGA nanoparticles loaded capecitabine for prostate cancer, International journal of clinical and experimental medicine 8(10) (2015) 19670-81.
69. L.T.M. Phuc, A. Taniguchi, Epidermal Growth Factor Enhances Cellular Uptake of Polystyrene Nanoparticles by Clathrin-Mediated Endocytosis, International journal of molecular sciences 18(6) (2017).
70. S. Pandey, M.S. Vijayendra Swamy, M.U. Ubaid Ulla, A. Gupta, H. Patel, S.J. Yadav, Cell Line and Augument Cellular Uptake Study of Statistically Optimized Sustained Release Capecitabine Loaded Eudragit S100/PLGA(poly(lacticco- glycolic acid)) Nanoparticles for Colon Targeting, Current Drug Delivery 14(6) (2017) 887-899.

71. J. Du, J. Xu, J. Chen, W. Liu, P. Wang, K. Ye, circRAE1 promotes colorectal cancer cell migration and invasion by modulating miR-338-3p/TYRO3 axis, Cancer cell international 20 (2020) 430.
72. N. Clemente, M. Argenziano, C.L. Gigliotti, B. Ferrara, E. Boggio, A. Chiocchetti, F. Caldera, F. Trotta, E. Benetti, L. Annaratone, S. Ribero, S. Pizzimenti, G. Barrera, U. Dianzani, R. Cavalli, C. Dianzani, Paclitaxel-Loaded Nanosponges Inhibit Growth and Angiogenesis in Melanoma Cell Models, Frontiers in pharmacology 10 (2019) 776.
73. S. Haque, C.C. Norbert, R. Acharyya, S. Mukherjee, M. Kathirvel, C.R. Patra, Biosynthesized Silver Nanoparticles for Cancer Therapy and In Vivo Bioimaging, Cancers 13(23) (2021).
74. A.Y. Sherif, G.I. Harisa, F.K. Alanazi, F.A. Nasr, A.S. Alqahtani, Engineered Nanoscale Lipid-Based Formulation as Potential Enhancer of Gefitinib Lymphatic Delivery: Cytotoxicity and Apoptotic Studies Against the A549 Cell Line, AAPS PharmSciTech 23(6) (2022) 183.

Tables

Table 1: Profile of particle size, zeta potential, loading efficiency, cumulative drug release at 100th Hr of prepared nanoparticles

Formulation name	Particle Size (nm)	Zeta potential (mV)	Loading efficiency (%) at 10µg/mL concentration	Cumulative drug release % at 100th hours
Capecitabine (CTB)	-	-	-	>100
PS-NPs	171±17.78	+7.3±1.09	-	-
CTB-PS-NPs	190±10.67	+10.3±2.09	22.45±1.85	100.178±5.78
CS-NPs	191±17.33	+21.3±4.09	-	-
CTB-CS-NPs	196±12.78	+27.3±4.09	52.45±2.85	97.78±5.78
PS-CS-NPs	194±19.45	+28.7±7.15	-	-
CTB-PS-CS-NPs	245±10.45	+30.3±8.09	76.45±3.85	92.25±5.78

CTB-Capecitabine**; PS-** Potato Starch; **CS-**Chitosan; **NPs-** Nanoparticles

Table 2: IC_{50} of pure CTB, CTB-CS-NPs, CTB-PS-NPs, CTB-PS-CS-NPs at 24th hour, 48th hours on cell viability of HT-29 cells line using MTT assay

Duration	Pure CTB (µg/mL)	CTB-CS-NPs (µg/mL)	CTB-PS-NPs (µg/mL)	CTB-PS-CS-NPs (µg/mL)
24th hr	23.45±0.63	15.56±0.93	14.56±0.90	10.10±0.22
48th hr	14.36±0.53	8.72±1.03	7.22±1.22	5.20±0.71

Table 3: Outcomes of crystal violet assay

	HT-29
CTB 10^{-7} M	16.4 ± 5.7
CTB 10^{-8} M	12.4 ± 4.3
CTB 10^{-9} M	10.8 ± 4.3
CTB-CS-NPs 10^{-10} M	15.2 ± 3.4
CTB-CS-NPs 10^{-11} M	10.4 ± 6.4
CTB-CS-NPs 10^{-12} M	7.5 ± 5.2
CTB-PS-NPs 10^{-10} M	12.4 ± 4.3
CTB-PS-NPs 10^{-11} M	9.6 ± 3.1
CTB-PS-NPs 10^{-12} M	8.4 ± 5.2
CTB-PS-CS-NPs 10^{-10} M	9.8 ± 2.4
CTB-PS-CS-NPs 10^{-11} M	6.4 ± 4.1
CTB-PS-CS-NPs 10^{-12} M	4.3 ± 3.2

Figures

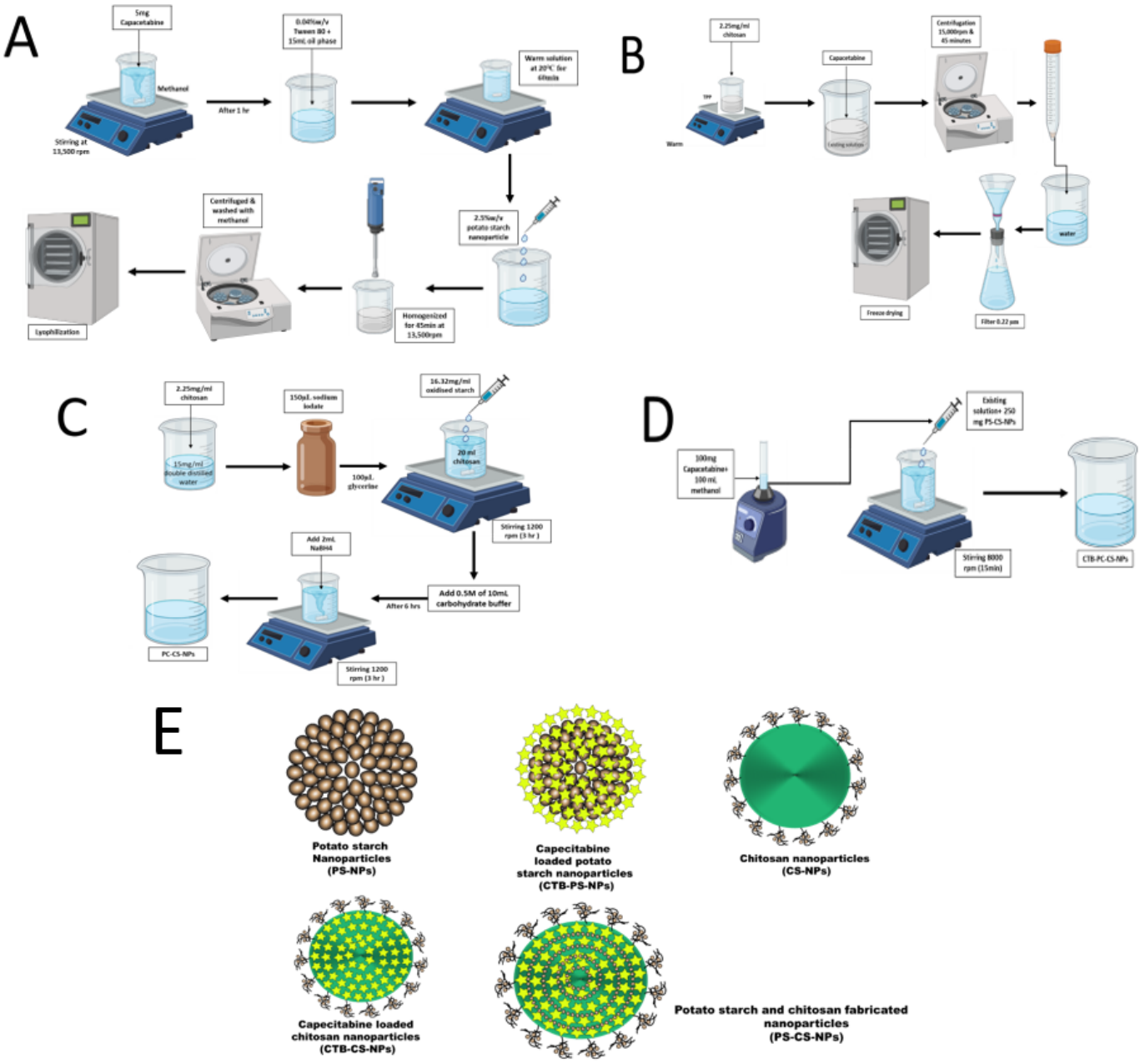

Figure 1

(A) Capacetabine loaded potato starch nanoparticles. **(B)** Capacetabine loaded chitosan nanoparticles. **(C)**Preparation of potato starch & chitosan fabricated nanoparticles. **(D)**Preparation of Capecitabine loaded potato starch and chitosan fabricated nanoparticles. **(E)** Hypothetical representation of different types of polymeric nanoparticles comprising potato starch and chitosan.

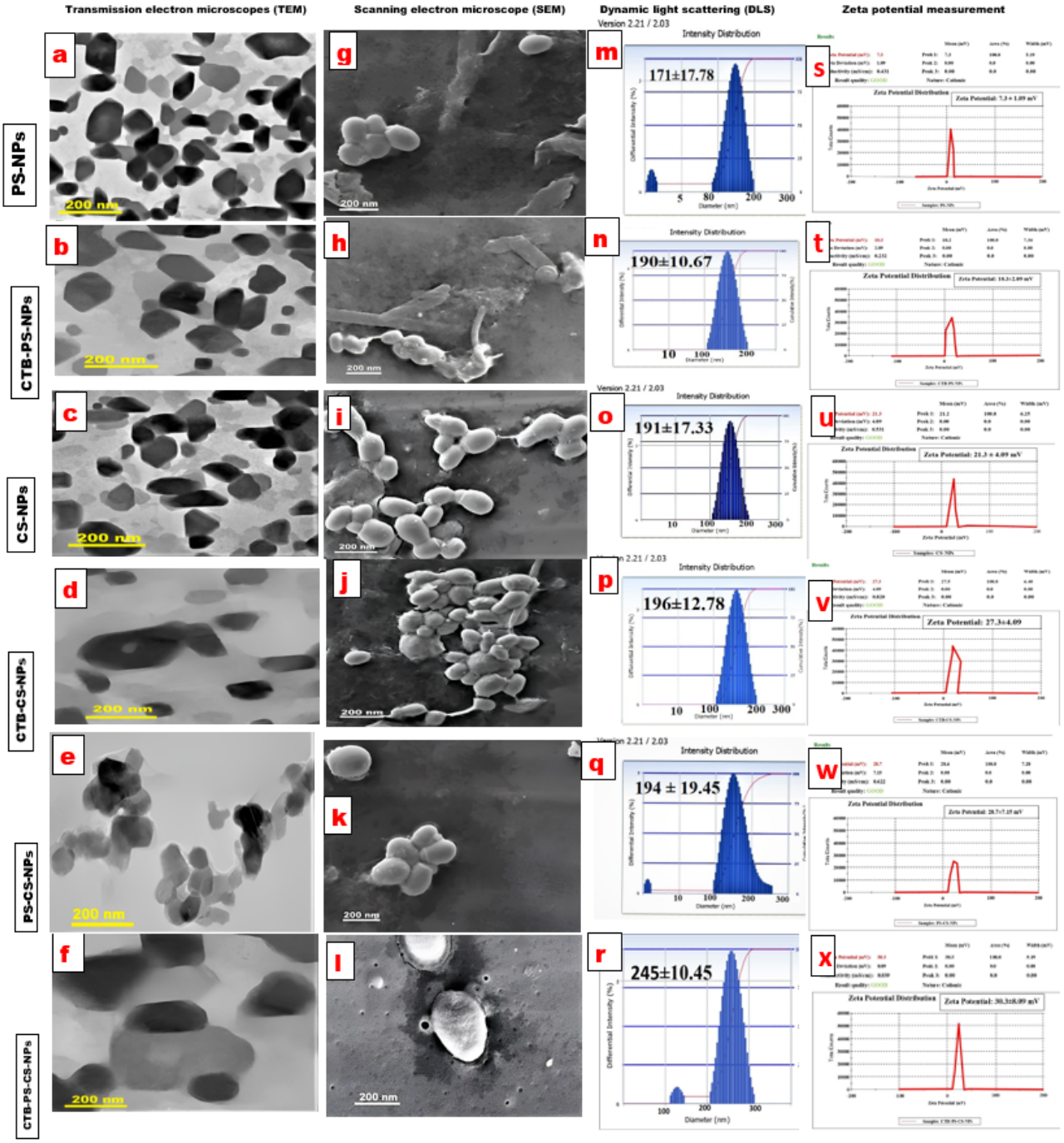

Figure 2

Scanning electron microscopy images of (a) PS-NPs, (b) CTB-PS-NPs, (c) CS-NPs, (d) CTB-CS-NPs, (e) PS-CS-NPs, (f) CTB-PS-CS-NPs, and transmission electron microscope images of (g) PS-NPs, (h) CTB-PS-NPs, (i) CS-NPs, (j) CTB-CS-NPs, (k) PS-CS-NPs, (l) CTB-PS-CS-NPs. Particle size distributions of starch nanoparticles: (m) PS-NPs, (n) CTB-PS-NPs, (o) CS-NPs, (p) CTB-CS-NPs, (q) PS-CS-NPs, (r) CTB-PS-CS-NPs. Zeta potential of starch nanoparticles (s) PS-NPs, (t) CTB-PS-NPs, (u) CS-NPs, (v) CTB-CS-NPs, (w) PS-CS-NPs, (x) CTB-PS-CS-NPs

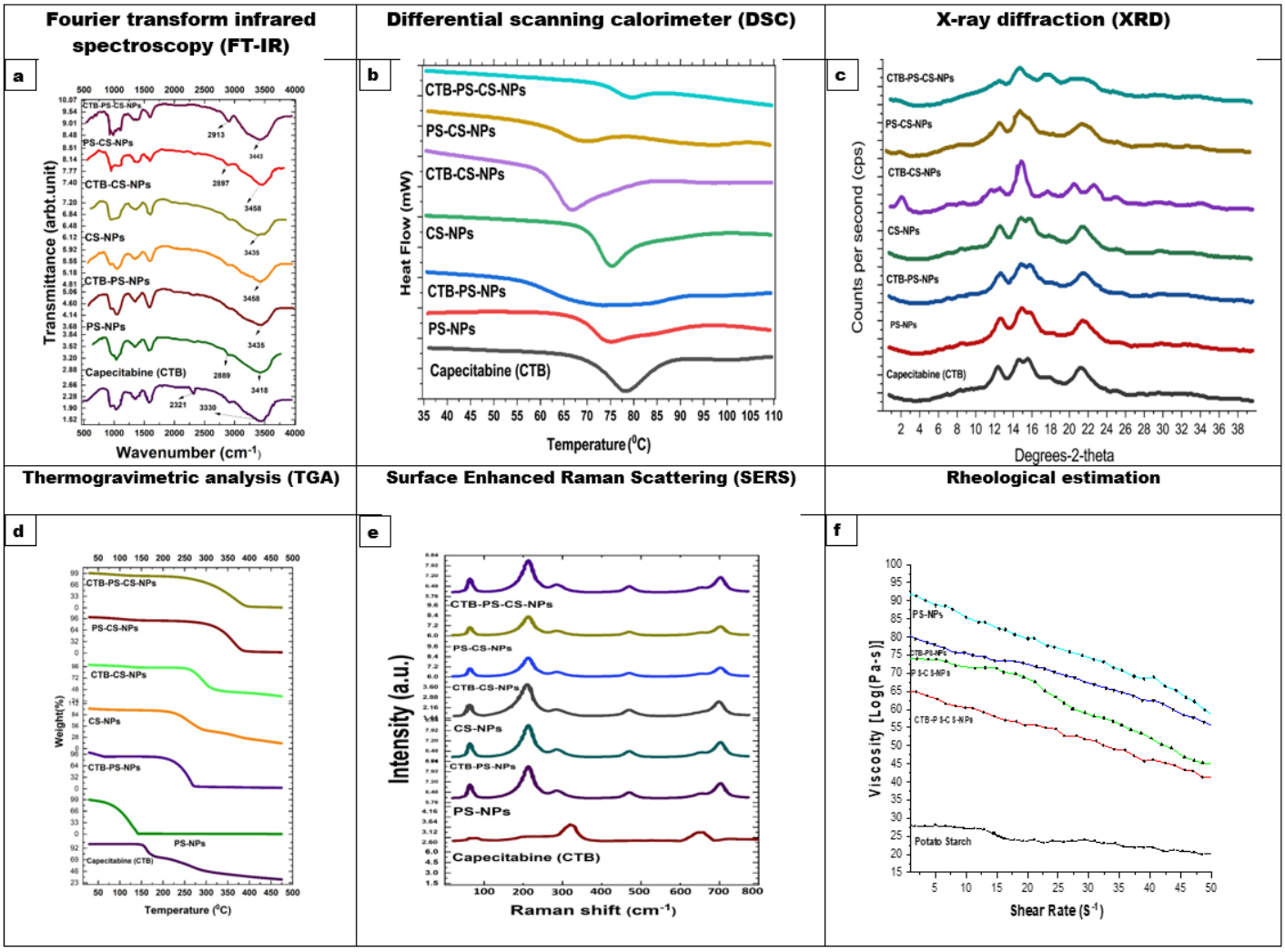

Figure 3

(a). Fourier transform infrared spectroscopy of CTB, PS-NPs, CTB-PS-NPs, CS-NPs, CTB-CS-NPs, PS-CS-NPs, CTB-PS-CS-NPs **(b).** Differential scanning calorimetry thermograms CTB, PS-NPs, CTB-PS-NPs, CS-NPs, CTB-CS-NPs, PS-CS-NPs, CTB-PS-CS-NPs **(c).** X-ray diffraction patterns of CTB, PS-NPs, CTB-PS-NPs, CS-NPs, CTB-CS-NPs, PS-CS-NPs, CTB-PS-CS-NPs **(d).** thermogravimetric analysis curves of CTB, PS-NPs, CTB-PS-NPs, CS-NPs, CTB-CS-NPs, PS-CS-NPs, CTB-PS-CS-NPs. **(e)** The anti-symmetric vibration from the lactic unit, which is constrained to a lesser intensity in the PS and CS loaded Nanoparticles group, is suggested by the Raman spectra at 200 cm^{-1} for PS-NPs, CTB-PS-NPs, CS-NPs, CTB-CS-NPs, PS-CS-NPs, and CTB-PS-CS-NPs. **(f)** Viscosity of potato starch (PS) and PS nano starch particles against shear rate.

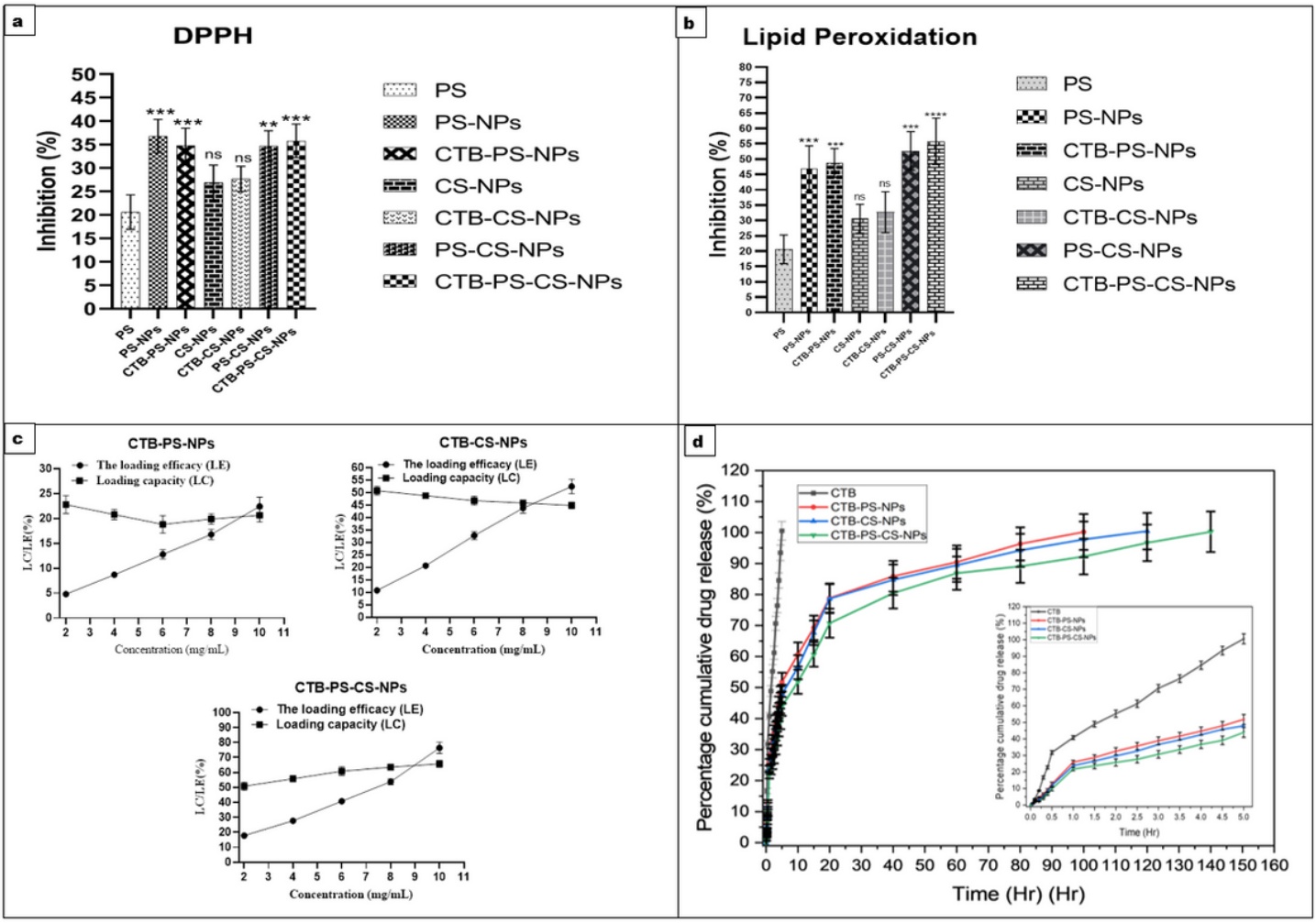

Figure 4

Antioxidant analysis of native and nano starch particles. **(a)** represents DPPH (2,2-diphenyl-1-picryl-hydrazyl-hydrate) assay. **(b).** Lipid peroxidation assay. Data with different superscript above the bars are significantly different ($p < 0.05$). **(c).** The loading efficacy (LE) and the loading capacity (LC) of CTB-PS-NPs, CTB-CS-NPs and CTB-PS-CS-NPs **(d).**percentage cumulative drug release profile of Capecitabine (CTB) and CTB loaded nanoparticles

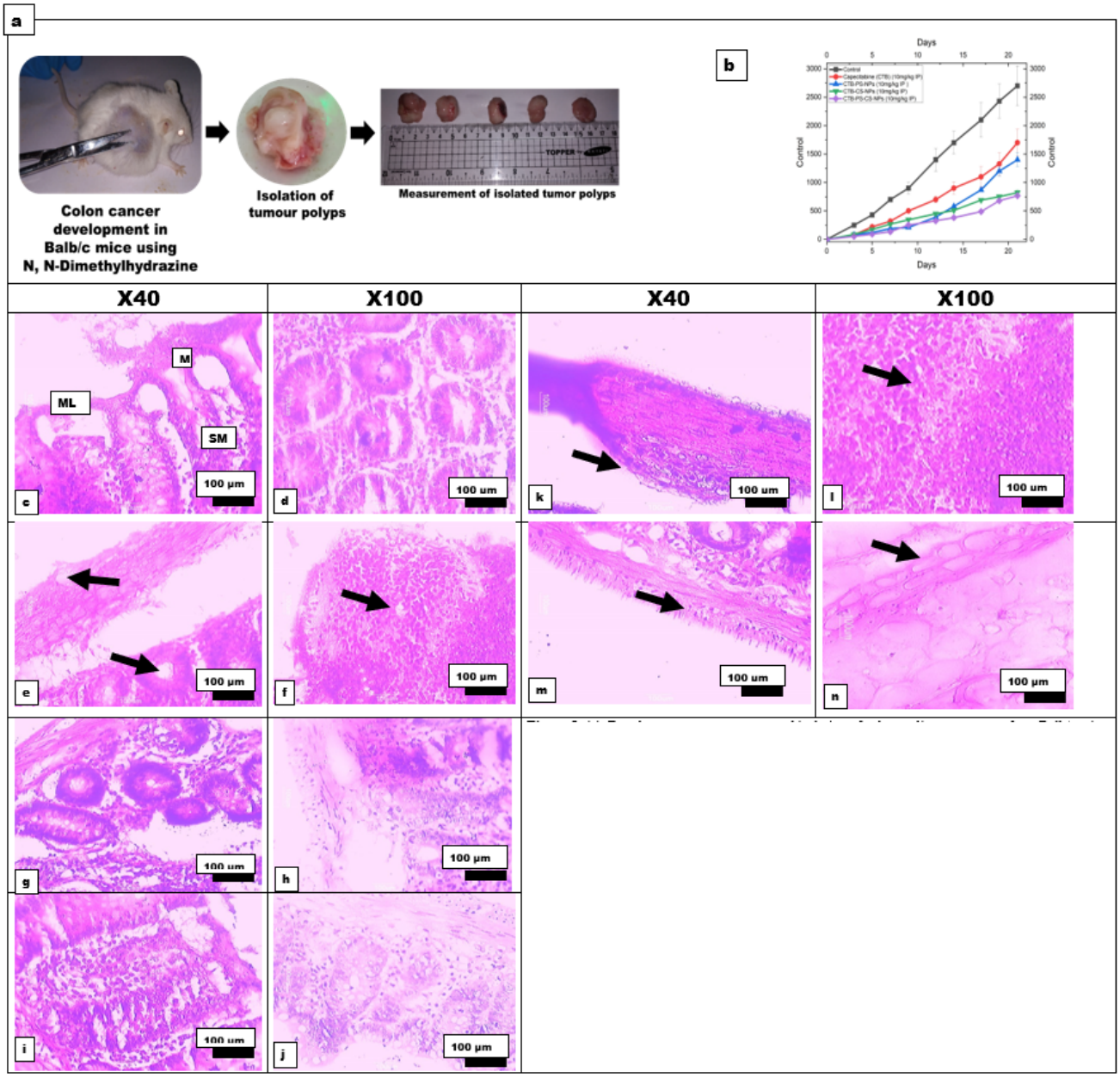

Figure 5

(a). Development, measurement, and isolation of colon malignant tumours from Balb/c mice. **(b).** Tumour regression study in N, N-Dimethylhydrazine (DMH) model showing changes in relative tumour volume with time (days) of different groups Balb/c mice (n=6) treated with CTB and CTB-loaded CTB-PS-NPs, CTB-CS-NPs, and CTB-PS-CS-NPs daily from week 12 to week 17 intraperitoneally (IP) 10mg/kg. injection. Hematoxylin and eosin-stained colonic sections showing histopathological changes **(c, d)** show normal mucosal layers **(M)**, submucosa **(SM)**, and musculus **(ML)** of the saline group.

The mucosal surface has integral columnar epithelium with acidophilic cytoplasm and oval nuclei at the bottom, flask-shaped goblet cells with vacuolated cytoplasm and flattened nuclei at the bottom, normal-shaped crypts with narrow openings, and normal connective tissue of the lamina propria between the crypts **(e, f)**show the hyperplastic, distorted mucosa of the DMH group, which is made up of improperly packed cells with hyperchromatic nuclei (black arrow), disintegrated goblet cells, morphologically changed crypts, and lamina propria with inflammatory cell infiltration. **(g, h)** show how architecture is messed up CTB; the group that was given 10 mg/kg had some moderate (grade 2) dysplasia, a lot of goblet cells, and some mild inflammatory cell infiltration between the crypts. The 10 mg/kg CTB-PS-NPs group **(i, j)** has moderate dysplasia (grade 2) and a moderate number of goblet cells. The crypts and submucosa of the 10 mg/kg CTB-CS-NPs (k,l) and 10 mg/kg CTB-PS-CS-NPs **(m, n)**groups are almost the same as normal. The H&E stain at X40 bar 100μm and X100 bar 100 μm.

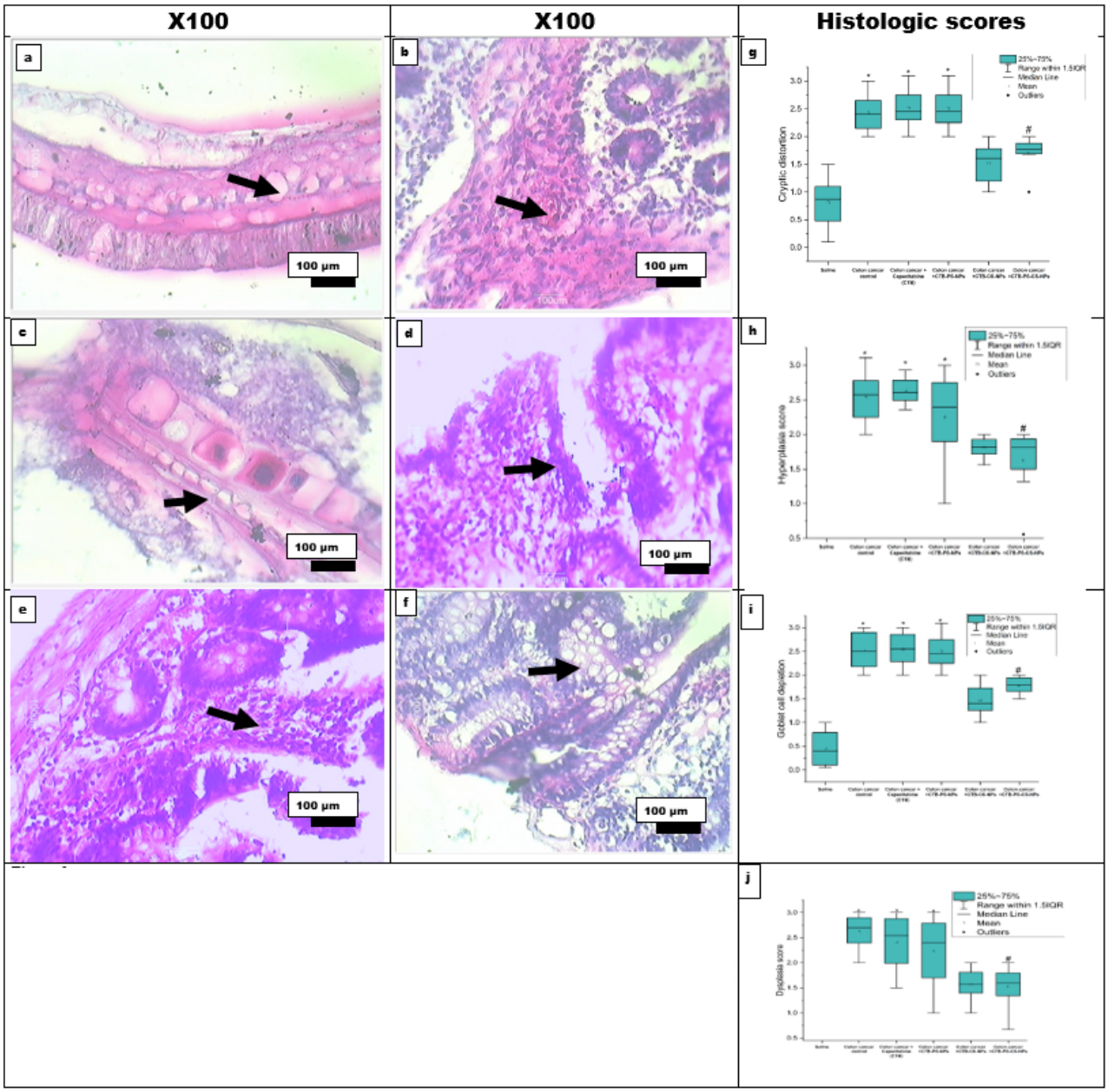

Figure 6

In the negative control group **(a)**, only a few chronic inflammatory cells can be seen in H&E-stained colonic microscopic sections. On the other hand, the DMH group **(b)** has a clear inflammatory infiltrate and lymphoid follicles that stand out (arrows). In the CTB 10 mg/kg group **(c)**, there was moderate inflammation with lymphoid aggregates. In the CTB-PS-NPs 10 mg/kg group **(d)**, there was mild inflammation with small lymphoid aggregates, and in the CTB-CS-NPs 10 mg/kg group **(e)**, there were few inflammatory cells recorded in CTB-PS-CS-NPs 10 mg/kg group (f). H&E stain magnifications: X100 bar 100 µm. Colon samples stained with H&E and given histologic scores: **(g)** Cryptic distortion, **(h)**hyperplasia, I goblet cell depletion, and **(j)** dysplasia. An experienced pathologist gave each item a

score between 0 to 3. Kruskal-Wallis ANOVA and Dunn's post hoc test were used to compare different groups when p < 0.05 *: versus saline group, #: versus colon cancer control group, p < 0.05.

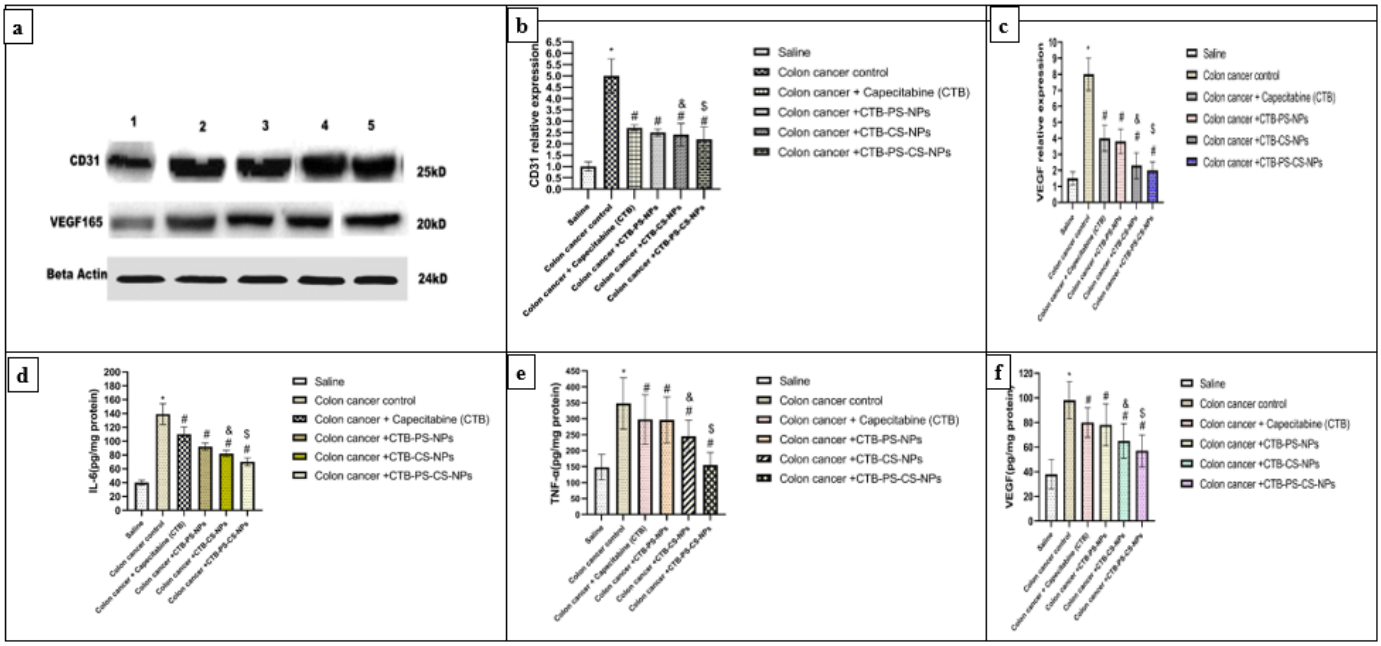

Figure 7

VEGF and CD31 were detected using western blotting in colon cancer model **(a)** Western blots were performed to look for the proteins CD31, VEGF, and β-actin. 1: saline, 2: DMH, 3: saline, 4,5: DMH+ Capecitabine (CTB) 10mg/kg. **(b & c)** column charts for mean ± SD for density of CD31 and VEGF for DMH + CTB-PS-NPs 10 mg/kg, DMH +CTB-CS-NPs 10 mg/kg, and DMH +CTB-PS-CS-NPs 10 mg/kg, respectively. *: in comparison to the saline group; #: in contrast to the colon cancer control group; and &: in contrast to the colon cancer group treated with capecitabine (CTB) 10 mg/kg and $: against colon cancer when combined with CTB-PS-NPs, CTB-CS-NPs, and CTB-PS-CS-NPs at a dose of 10 mg/kg, p<0.05. Level of the proangiogenic components in the colon homogenates of the experimental groups. **(d)** IL-6, **(e)** TNF-α and **(f)**VEGF. *: versus saline group, #: versus colon cancer control group, &: versus colon cancer + Capecitabine (CTB) 10 mg/kg and $: versus colon cancer + CTB-PS-NPs, CTB-CS-NPs, and CTB-PS-CS-NPs 10 mg/kg, p < 0.05.

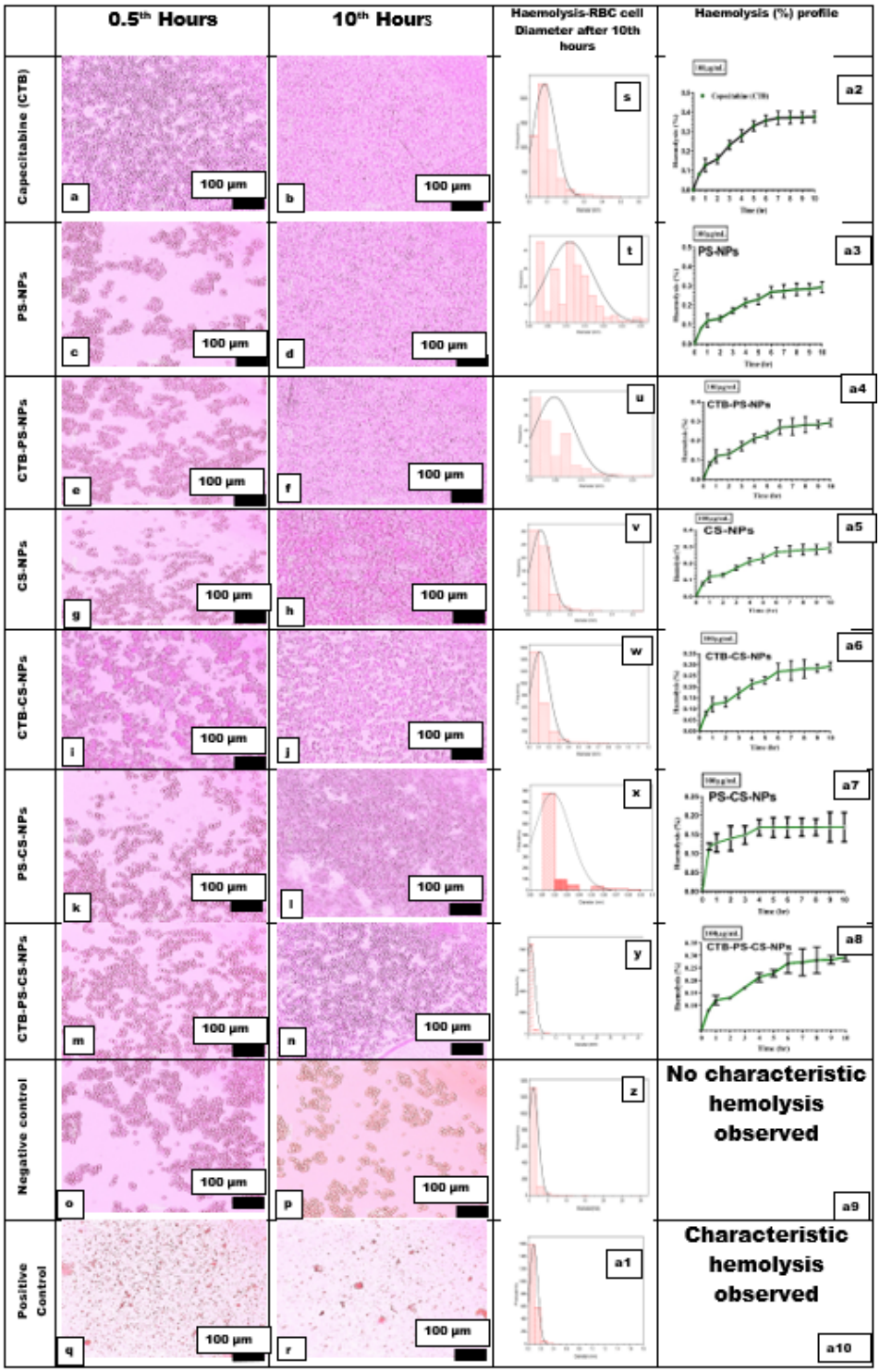

Figure 8

High contrast microscopic images of erythrocytes during haemolysis (%) studies after 100µg/mL of Capecitabine (CTB) **(a, b)**, PS-NPs **(c, d)**, CTB-PS-NPs **(e, f)**, CS-NPs **(g, h)**, CTB-CS-NPs **(i, j)**, PS-CS-NPs **(k. l)**, CTB-PS-CS-NPs **(m. n)** with pH 6.8 PBS solution treatment (negative controlled) **(o. p)** and Triton X-100 treatment (positive controlled) **(q, r)** during the 0.5th and 10th hours. For each treatment. The cell diameter (nm) and cell frequency were measured after 10 hours of intravenous administration. For all the

batches the haemolysis diameters were recorded **(s-a1)** and further, haemolysis (%) profile has been recorded **(a2 -a8)**, except positive control and

negative control group.

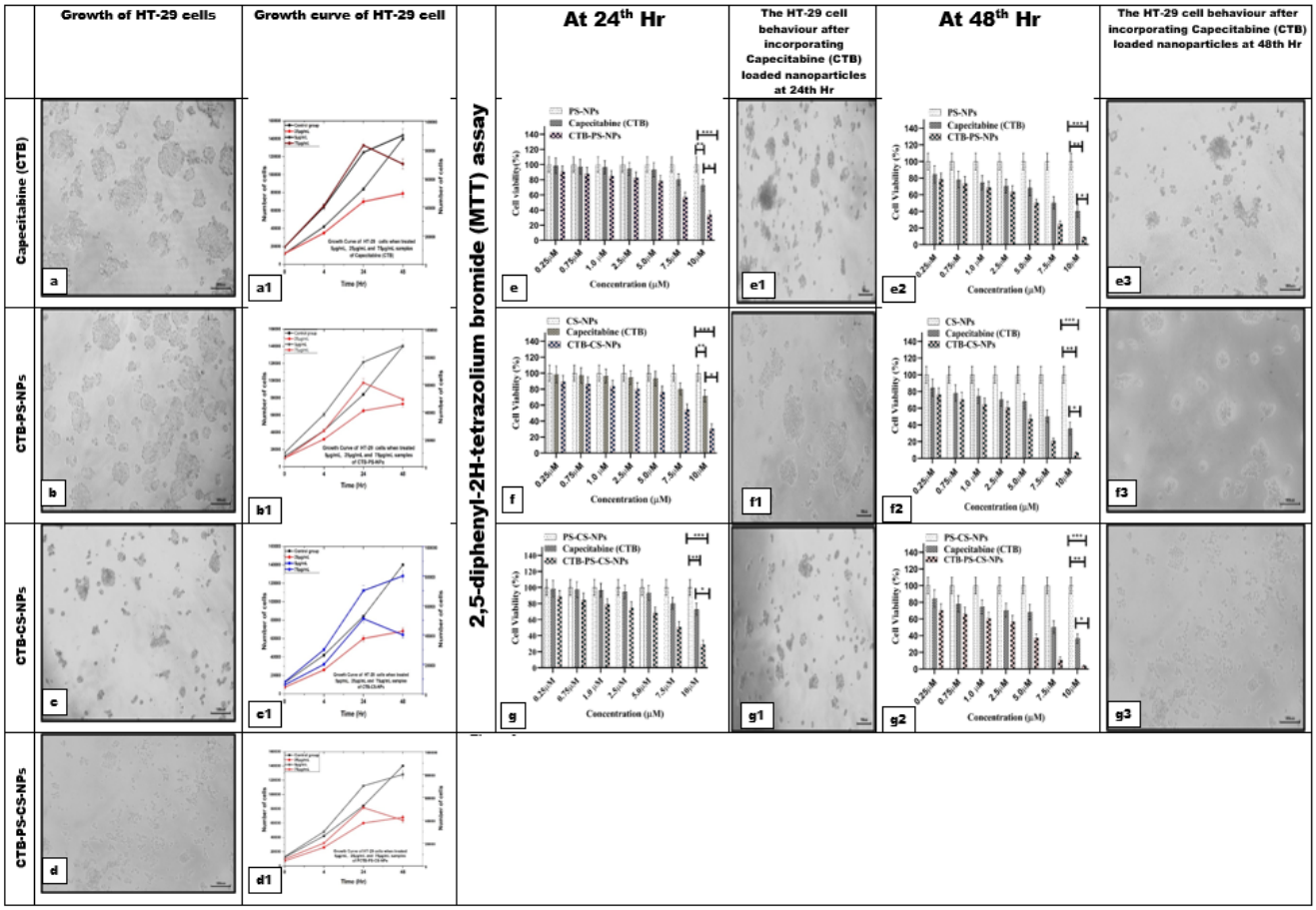

Figure 9

Growth curve in the HT-29 cells was determined by Trypan Blue (counting dye method). The effects of Capecitabine (CTB), CTB-PS-NPs, CTB-CS-NPs,

CTB-PS-CS-NPs exposure were evaluated at 4, 24, and 48 h at 5, 25, and 75 µg/mL concentrations and compared to the control cells. Microscopic images of HT-29 cell growth with Capecitabine (CTB) **(a)**, CTB-PS-NPs **(b)**, CTB-CS-NPs **(c)**, and CTB-PS-CS-NPs **(d)** at 75µg/mL, as well as their cell growth curve at all concentrations **(a1, b1, c1, d1)**. HT-29 cell growth was suppressed when 75µg/mL of CTB-PS-CS-NPs were added to the cells; indicating superior anticancer effects of CTB-PS-CS-NPs. Error bars represent the standard error of the mean. Cell viability studies of free Capecitabine (CTB), CTB-PS-NPs, CTB-CS-NPs, CTB-PS-CS-NPs, on HT-29 cell lines using MTT assay at 24th hours **(e–g)** & at 48th hours **(e2–g2)** (mean ± SD; n= 3, *p< 0.05, **p <0.01, ***p <0.001. The HT-29 cell behaviour was also can be seen after

incorporating Capecitabine (CTB), CTB-PS-NPs, CTB-CS-NPs, CTB-PS-CS-NPs at 24th **(e1, f1, g1)** and 48th hours **(e3, f3 and g3)**

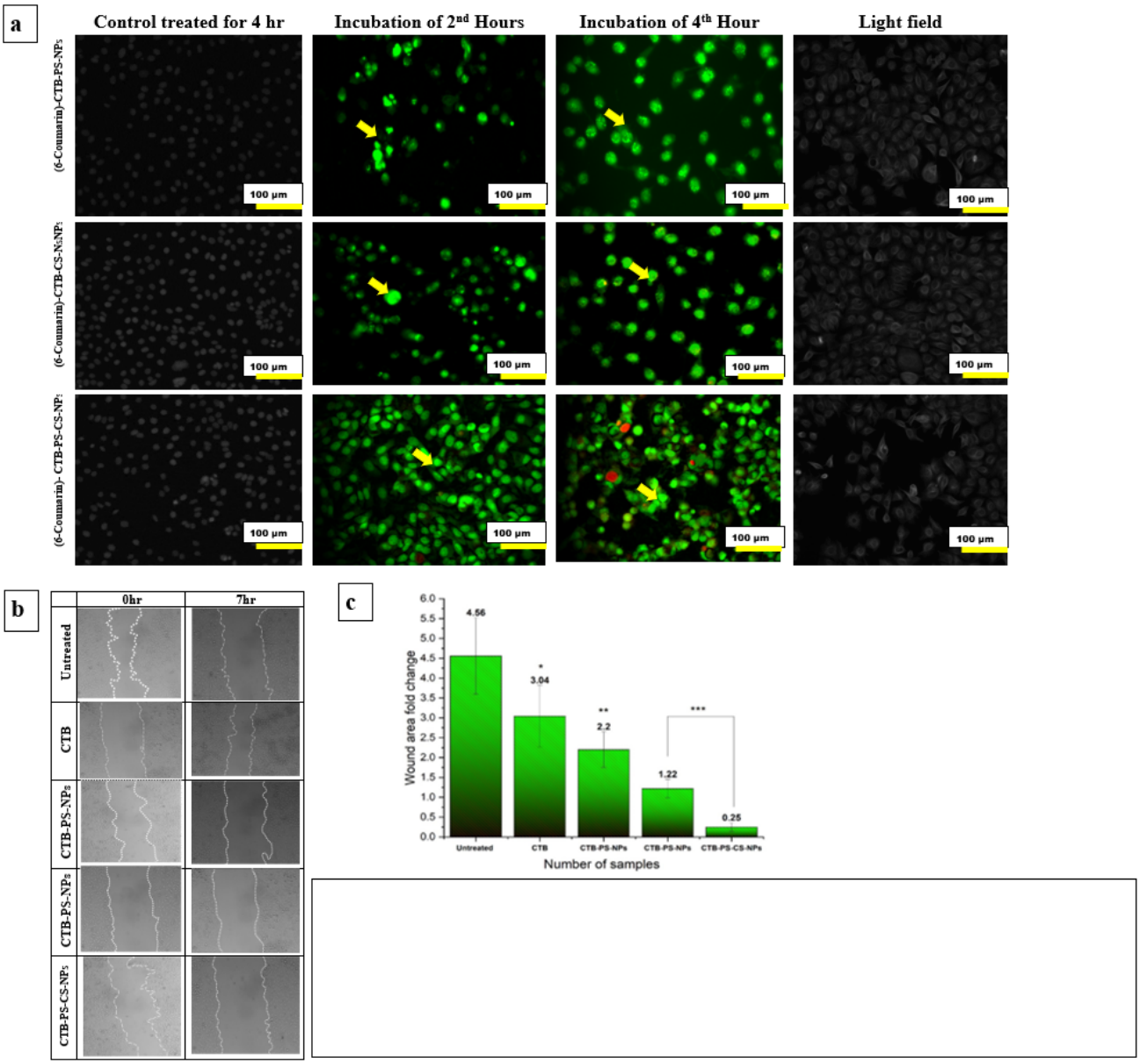

Figure 10

(a). Time-dependent intracellular accumulation of (6-Coumarin)-CTB-PS-NPs, (6-Coumarin)-CTB-CS-NPs, (6-Coumarin)-CTB-PS-CS-NPs, Control treated for 4 hr, Incubation of 2 hr, Incubation of 4 hr, and Light field images of 6-Coumarin loaded nanoparticles. Control treated for 4 hr, Incubation of 2 hr, Incubation of 4 hr, and Light field in HT-29 cells under confocal laser scanning fluorescence microscope. Yellow arrows indicate the higher uptake of 6-coumarin conjugated nanoparticles with compared to unconjugated nanoparticles at incubation of 2 hr and 4 hr. **(b**) Determination of wound healing of HT-29 cell lines for untreated (first row). The CTB inhibits the migration of cells (IC50: 4. µL =1.25 µg/mL) compared to untreated cells. **(c)** Histogram representation of healing of wound area is calculated using

Image J software which indicates less change in CTB-PS-NPs, CTB-CS-NPs, and CTB-PS-CS-NPs treated wound area as compared to the untreated sample. These experiments are performed thrice mean ± SD; n= 3, *p< 0.05, **p <0.01, ***p <0.001, where untreated group is considered as control.

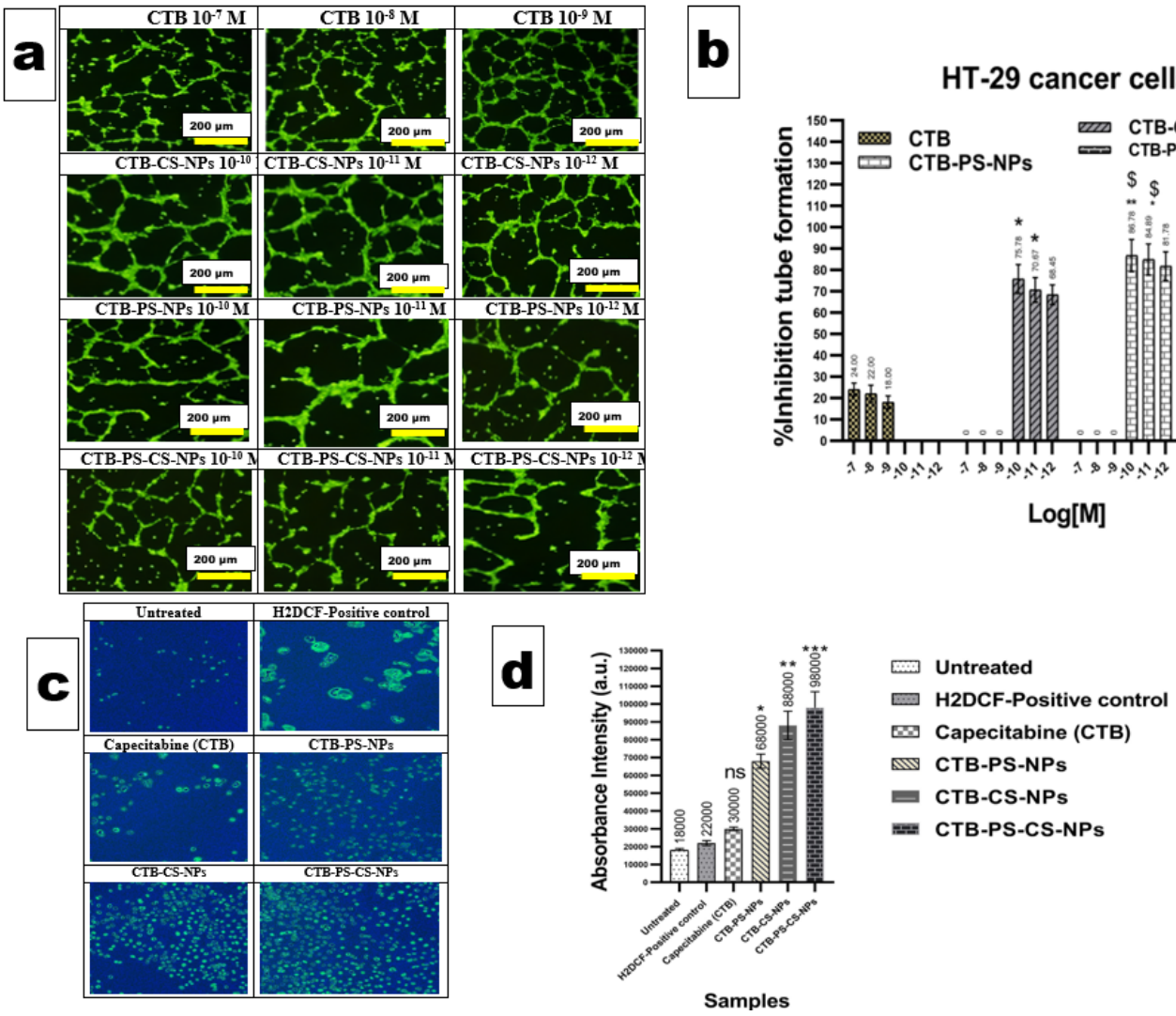

Figure 11

(a). Tube formation assay of HT-29 cells treated with different concentrations of Capecitabine (CTB), CTB-PS-NPs, CTB-CS-NPs, and CTB-PS-CS-NPs. HT-29 cells were plated in the presence and absence of CTB (from 10-7 to 10-9 M) and CTB-PS-NPs, CTB-CS-NPs, and CTB-PS-CS-NPs (from 10-10 to 10-12 M). The morphology of the capillary-like structures formed by the HT-29 cells was analyzed by an inverted microscope after 6 h of culture and photographed with a digital camera. **(b)**The graph shows the tube formation, evaluated by counting the total number of tubes in three wells of five different experiments. The results were expressed as % inhibition of untreated control cells. Data are expressed as mean ± SD. ∗∗p < 0.01, CTB vs CTB-PS-NPS, ∗p < 0.05, CTB vs CTB-CS-NPs, $$p < 0.01 Capecitabine (CTB) vs CTB-PS-CS-NPs $p < 0.05, CTB-PS-CS-NPs vs Capecitabine (CTB). **(c)** Determination of the intracellular ROS (H2O2) production in HT-29 cell line using 2',7'-dichlorodihydrofluorescein (H2DCF) reagent after

treatment with CTB, CTB-PS-NPs, CTB-CS-NPs and CTB-PS-CS-NPs and Tertiary-Butyl hydroperoxide: TBHP (positive control) for 5 h, **(d)** graphical representation of quantification of ROS generation. Higher amounts of hydrogen peroxide production is observed upon treatment with the CTB-PS-CS-NPs compared to untreated (UT) cells. These experiments are performed thrice mean ± SD; n= 3, *p< 0.05, **p <0.01, ***p <0.001, ns=non-significant, where untreated group is considered as control.

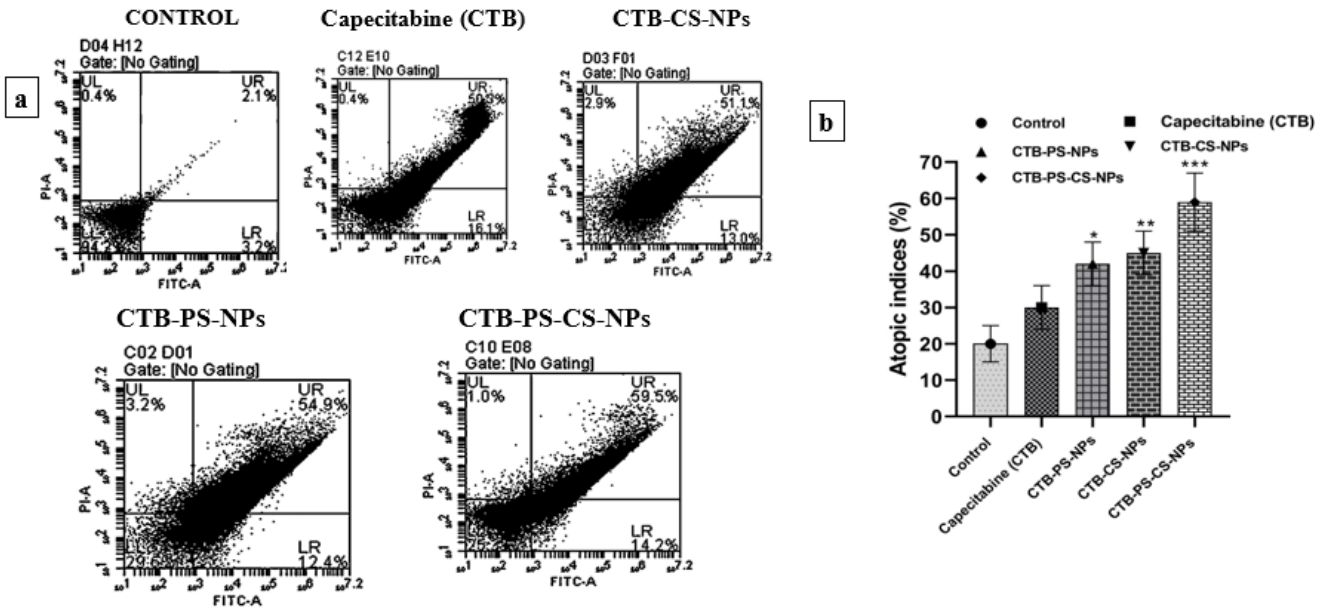

Figure 12

(a) CTB, CTB-CS-NPs, CTB-PS-NPs, CTB-PS-CS-NPs induces apoptosis in HT-29 cells. Single-cell suspensions were prepared from tumor tissues of control and treated groups as described in materials and methods. Apoptotic cells were determined by FITC Annexin-V staining and flow cytometry. The flow cytometric analyses are shown as histograms and the percentage of apoptotic cells are shown as bar graph. **(b)** Control group; Capecitabine (CTB)-treated group CTB-PS-NPs-treated group; CTB-CS-NPs-treated group; CTB-PS-CS-NPs–treated group in HT-29 cells. Statistical analyses were performed with Student's t-test. *p < 0.01 compared with control group. These experiments are performed thrice mean ± SD; n= 3, *p< 0.05, **p <0.01, ***p <0.001, where untreated group is considered as control.

Supplementary Files

This is a list of supplementary files associated with this preprint. Click to download.

- GA.png